

國立交通大學

電信工程研究所



強健性心電信號壓縮演算法之研究

**A Study of Noise-Resilient Compression Algorithm
for ECG Signals**

研究生：黎忠孝

指導教授：張文輝 博士

中華民國一百零二年六月

強健性心電信號壓縮演算法之研究
A Study of Noise-Resilient Compression Algorithm
for ECG Signals

研究生：黎忠孝

Student: Trung-Hieu Le

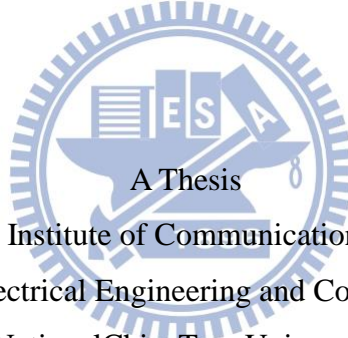
指導教授：張文輝

Advisor: Wen-Whei Chang

國立交通大學

電信工程研究所

碩士論文



Submitted to Institute of Communications Engineering
College of Electrical Engineering and Computer Science

National Chiao Tung University

in Partial Fulfillment of the Requirements

for the Degree of

Master

in

Communication Engineering

June 2013

Hsinchu, Taiwan, Republic of China

中華民國一百零二年六月

強健性心電信號壓縮演算法之研究

研究生：黎忠孝指導教授：張文輝

國立交通大學
電信工程研究所

摘要

因應高齡化社會的未來趨勢，遠距醫療與居家健康照護已經成為先進國家重點發展的新興服務產業。本論文旨在發展一高效能的心電信號壓縮演算法，以期長時間監測心臟機能的異常徵兆而防患於未然。演算法的設計需兼顧即時製作與強健性能，前者強調簡化運算得以快速實現，後者則要求訊源與量測雜訊能分離處理。第一項研究課題著重於理想傳輸環境下心電訊號壓縮演算法的設計。一維壓縮演算法是採用增益-形狀碼本結構的多層級向量量化機制，另一種是基於國際影像壓縮標準 JPEG2000 的二維壓縮演算法。第二項課題旨在探討能有效對抗環境雜訊干擾的信號除噪技術，其關鍵是參考希伯特-黃轉換理論而設計一兼顧時域及頻域非穩態特性的信號分析技術。針對 MIT-BIH 心電圖資料庫進行的系統模擬結果顯示，新的方法適用於行動心臟照護系統的未來應用。

關鍵字：心電信號壓縮，向量量化，小波，信號除噪，希伯特-黃轉換

A Study of Noise-Resilient Compression Algorithm for ECG Signals

Student: Le TrungHieu

Advisor: Dr. Wen-Whei Chang

Institute of Communications Engineering,
National Chiao Tung University
Hsinchu, Taiwan

Abstract

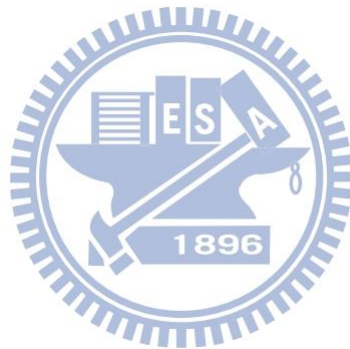
The volume of ECG data produced by monitoring systems can be quite large, and data compression is needed for efficient transmission over mobile networks. We first propose a new method based on the multiple stage vector quantization in conjunction with gain-shape codebooks. The compression of ECG signals using JPEG2000 is also investigated. The good time-frequency localization properties of wavelets make them especially suitable for ECG compression applications. Also proposed is a method of ECG signal denoising based on Hilbert-Huang transform. This method uses empirical mode decomposition to decompose the signal into several intrinsic mode functions (IMFs) and then the noisy IMFs are removed by using soft-threshold method. Experiments using the MIT-BIH arrhythmia database illustrate that the proposed approach has improved the performance at a high compression ratio.

Keywords: ECG compression, vector quantization, wavelets, signal denoising, Hilbert-Huang transform

Acknowledgements

I would like to acknowledge my advisors, Prof. Wen-Whei Chang, for his valuable guidance throughout my research. I would also like to thank the colleagues in Speech Communication Lab for their helpful suggestions and discussions.

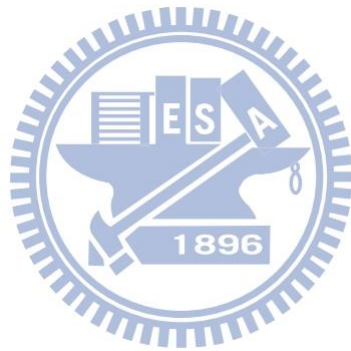
I would like to thank my parent for their belief and encouragement.



Contents

摘要.....	i
Abstract.....	ii
Acknowledgements.....	iii
Contents.....	iv
List of Figures.....	vi
List of Tables.....	viii
Chapter 1 Introduction.....	1
Chapter 2 Fundamental of ECG Signals.....	4
2.1 ECG characteristic.....	4
2.2 MIT-BIH ECG database.....	9
Chapter 3 Hilbert-Huang Transform for ECG Denoising.....	13
3.1 Hilbert-Huang Transform:.....	13
3.1.1 Empirical mode decomposition (EMD).....	13
3.1.2 Hilbert Transform:.....	15
3.2 HHT-based denoising.....	16
Chapter 4 VQ-based ECG Compression.....	18
4.1 Vector Quantization.....	18
4.2 VQ for ECG Compression.....	21
4.2.1 Gain-Shape Vector Quantization.....	21
4.2.2 Multistage VQ.....	25
Chapter 5 JPEG2000-Based ECG Compression.....	29
5.1 JPEG2000.....	29
5.2 JPEG2000 for ECG compression:.....	33
Chapter 6 Experimental Results.....	37
6.1 Preprocessing Data.....	37

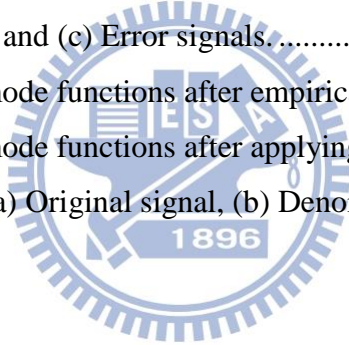
6.2	Experimental results of Algorithm I.....	38
6.3	Experimental results of Algorithm II	41
6.4	Experimental results of ECG denoising	46
Chapter 7	Conclusions.....	49
Bibliography	50



List of Figures

Figure 2.1	Typical cardiac cycle.....	5
Figure 2.2	Placements of electrodes.....	7
Figure 2.3	MIT-100 waveform.....	12
Figure 2.4	MIT-205 waveform.....	12
Figure 2.5	MIT-207 waveform.....	12
Figure 2.6	MIT-118.....	12
Figure 4.1	The VQ transmission system.....	20
Figure 4.2	VQ-based ECG compression.....	21
Figure 4.3	The gain-shape VQ system.....	22
Figure 4.4	Gain-shape VQ (a) encoder (b) decoder.....	25
Figure 4.5	The Two-Stage MSVQ system.....	26
Figure 4.6	The proposed ECG compression system: (a) the encoder, (b) the decoder.....	28
Figure 5.1	The block diagrams of JPEG2000 codec.....	30
Figure 5.2	Tiling, DC level shifting and DWT of each image tile component.....	31
Figure 5.3	flow-of-bit view of JPEG2000 encoder.....	32
Figure 5.4	Results obtained by progressive JPEG (P-JPEG), progressive JPEG2000 (both embedded lossless, R, and lossy, NR, versions) and MPEG-4 VTC baseline.[17].....	33
Figure 5.5	Block diagram of ECG encoder using JPEG2000.....	34
Figure 5.6	Block diagram of a ECG decoder using JPEG2000.....	34
Figure 5.7	Detection of ECG cycles.....	35
Figure 5.8	Before period normalization.....	36
Figure 5.9	After period normalization.....	36
Figure 6.1	Results of Algorithm I ($k = 8$) in MIT-BIH 100: (a) original signal, (b) reconstructed ECG waveforms, and (c) error signals.....	39
Figure 6.2	Results of Algorithm I ($k = 8$) in MIT-BIH 119: (a) original signal, (b) reconstructed ECG waveforms, and (c) error signals.....	39
Figure 6.3	Results of Algorithm I ($k = 8$) in MIT-BIH 122: (a) original signal, (b) reconstructed ECG waveforms, and (c) error signals.....	40
Figure 6.4	Results of Algorithm I ($k = 15$) in MIT-BIH 100: (a) original signal, (b) reconstructed ECG waveforms, and (c) error signals.....	40
Figure 6.5	Results of Algorithm I ($k = 15$) in MIT-BIH 119: (a) original signal, (b)	

reconstructed ECG waveforms, and (c) error signals.	40
Figure 6.6 Results of Algorithm I ($k = 15$) in MIT-BIH 122: (a) original signal, (b) reconstructed ECG waveforms, and (c) error signals.	41
Figure 6.7 MIT-100: (a) Original matrixes, (b) After period-normalization matrixes	42
Figure 6.8 MIT-108: (a) Original matrixes, (b) After period-normalization matrixes	43
Figure 6.9 MIT-119: (a) Original matrixes, (b) After period-normalization matrixes	43
Figure 6.10 MIT-122: (a) Original matrixes, (b) After period-normalization matrixes	44
Figure 6.11 Results of Algorithm II in MIT-BIH 100: (a) Original signal, (b) Reconstructed ECG waveforms, and (c) Error signals.	44
Figure 6.12 Results of Algorithm II in MIT-BIH 108: (a) Original signal, (b) Reconstructed ECG waveforms, and (c) Error signals.	45
Figure 6.13 Results of Algorithm II in MIT-BIH 119: (a) Original signal, (b) Reconstructed ECG waveforms, and (c) Error signals.	45
Figure 6.14 Results of Algorithm II in MIT-BIH 122: (a) Original signal, (b) Reconstructed ECG waveforms, and (c) Error signals.	45
Figure 6.15 Eight intrinsic mode functions after empirical mode decomposition	47
Figure 6.16 Eight intrinsic mode functions after applying soft threshold	47
Figure 6.17 MIT-BIH 108: (a) Original signal, (b) Denoised signal	48



List of Tables

Table 1.1	World’s top ten causes of death (2008) - WHO	1
Table 2.1	Descriptions of waves and durations.	6
Table 2.2	Placements of electrodes	7
Table 2.3	Beat annotations:.....	10
Table 2.4	Non-beat annotations:	11
Table 6.1	Performance results of Algorithm I.....	39
Table 6.2	Performance results of Algorithm II	42



Chapter 1 Introduction

Wireless patient monitoring has been of recent interest to researchers aiming to develop ubiquitous health-care systems able to provide personalized medical treatment continuously and remotely. To realize such systems, physiological signals such as ECG are measured and transmitted wirelessly to the remote server. Due to the limited bandwidth of transmission channel, ECG signal compression methods are used to reduce the large amount of data.

Every country in the world is aging with an increase of senior populations. With the increase of the elderly (65 years and over), the health-care issues are becoming more and more significant. Although traditional medical treatments such as face-to-face consultant cannot be replaced, some treatments can be done more efficiently with the biotelemetry. According to Table 1.1, heart diseases account for 12.8% of all deaths in 2008. The ECG is a graphical representation of the electrical activity in the heart and is useful for cardiac disease diagnosis. This motivates the research in designing an ECG monitoring system which can compress and transmit the ECG signals to the hospital or clinical center.

Table 1.1 World's top ten causes of death (2008) - WHO

World	Deaths in millions	% of deaths
Ischaemic heart disease	7.25	12.8%
Stroke and other cerebrovascular disease	6.15	10.8%
Lower respiratory infections	3.46	6.1%
Chronic obstructive pulmonary disease	3.28	5.8%
Diarrhoeal diseases	2.46	4.3%
HIV/AIDS	1.78	3.1%
Trachea, bronchus, lung cancers	1.39	2.4%
Tuberculosis	1.34	2.4%
Diabetes mellitus	1.26	2.2%
Road traffic accidents	1.21	2.1%

With the advanced development of mobile cellular network, more services can be provided for home health-care applications. A coding technique that provides channel efficiency is needed because it helps reduce resources usage, such as data storage space or

transmission capacity. This thesis first applies the Hilbert-Huang Transform as a method to ECG signal denoising. One dimensional ECG compression is achieved by using the Multistage Vector quantization (MSVQ) together with Gain-shape codebooks. Also proposed is a compression scheme based on JPEG2000, a well-established standard for compression of still images.

ECG signals are often corrupted by some noise during the measurement. The main interferences include baseline drift, electromyography, interference and frequency interference. Since ECG is very weak compared to noise, digital signal processing methods used for signal denoising are necessary. Previous research suggests the use of Hilbert-Huang Transform for noise filtering and denoising. The empirical mode decomposition (EMD) and the associated Hilbert transform, together designated as the Hilbert-Huang Transformation (HHT), are discussed in this work. The expansion of ECG data via the EMD method only has only a limited number of intrinsic mode functions (IMFs). Since the smaller scale IMFs can be considered as noise-dominated components, soft-threshold denoising methods can be used to remove the most noisy IMFs.

Most of the existing ECG compression methods adopt one-dimensional (1-D) representations for ECG signals, including direct waveform coding, transform coding, and parameter extraction methods. However, since the ECG signals have both sample-to-sample (intra-beat) and beat-to-beat (inter-beat) correlation, some 2-D compression techniques have been proposed for higher compression ratios [27,28]. These methods start with a preprocess procedure that converts 1-D to 2-D representations through the combined use of QRS detection and period normalization. Afterwards, the conventional image codec such as the JPEG standard can be used to compress these resulting 2-D arrays. JPEG2000 is the latest international standard for compression of still images. Although the JPEG2000 codec is designed to compress images, we illustrate that it can also be used to compress other signals.

In this thesis, we illustrate how the JPEG2000 codec can be used to compress electrocardiogram (ECG) data. In addition, this work also proposes a method based on multiple stage vector quantization (MSVQ) in conjunction with gain-shape codebook structure. We will evaluate the performances of the proposed schemes by using the ECG records from the MIT-BIH arrhythmia database.

This thesis is organized as follows. In Chapter 2, the fundamental of ECG signal will be reviewed, including the characteristic of ECG and the MIT-BIH database. Chapter 3 introduces the HHT algorithm and using HHT for denoising. Chapter 4 represents VQ-based compression, including GSVQ and MSVQ. Chapter 5 is derived by using JPEG2000 compression codec on ECG signals. Chapter 6 and Chapter 7 give the results of experiments and conclusion.



Chapter 2 Fundamental of ECG Signals

Electrocardiography(ECG) is a transthoracic (across the thorax or chest) interpretation of the electrical activity of the heart over a period of time, as detected by electrodes attached to the surface of the skin and recorded by a device external to the body. The recording produced by this noninvasive procedure is termed an ECG. ECG is commonly used to measure the rate and regularity of heartbeats, as well as the size and position of the chambers, the presence of any damage to the heart, and the effects of drugs or devices used to regulate the heart, such as a pacemaker. The ECG sources used in this research are acquired by using an open MIT-BIH database. In this chapter, introduction of ECG measurement and the ECG MIT-BIH sources used in our work are discussed.

2.1 ECG characteristic

Goal of an ECG device is to detect, amplify, and record the electrical changes caused by depolarization and repolarization of heart muscle. Each heart muscle cell, at rest condition, has a negative charge across its cell membrane and is called polarized. The negative charge can be increased to zero, and the phenomenon of depolarization causes the heart to contract. Afterwards, the heart muscle cell will be recharged, called repolarization, which makes the heart to expand. A cardiac cycle begins when the sinoatrial node (SA) generates the impulse, which will run through the heart. The conducting system of the heart can be summarized as follows:

1. The impulse generated from SA node will signal the muscle in the atria to beat, resulting in contraction, during which the blood is pushed from atria into ventricles.
2. The impulse propagates to atrioventricular(AV) node and then delays for about 1 millisecond to allow the blood to fill the ventricles.

3. The impulse propagates to the ventricles through the right bundle branch (RBB), the left bundle branch (LBB), and other nerves. This results in the ventricular contraction, during which the blood is pushed to the body.
4. The muscle cells are recharged (repolarization) and it expands the atrial so that the blood is allowed to return to the heart. Then, the next heartbeat repeats.

A typical cardiac cycle (ECG cycle) is composed of a P wave, a QRS complex, and a T wave. In addition, there are U wave and J wave within an ECG cycle, but their amplitudes are so low that they are often ignored. Different types of wave reflect the different stages of the heartbeats. A detailed description of each wave and its duration are shown in Fig 2.1 and Table 2.1. ECG is the most important tool to diagnose any damage to the heart. Symptoms like arrhythmia and myocardial infarction can be easily detected through ECG. For example, hyperacute T waves indicate that acute myocardial infarction may occur.

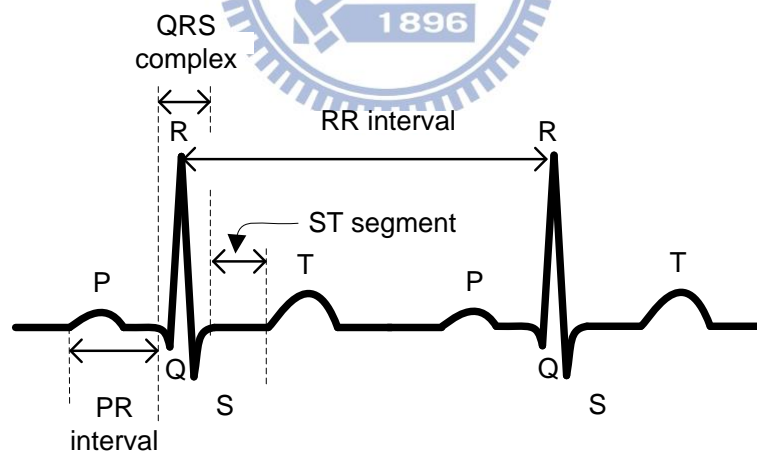


Figure 2.1 Typical cardiac cycle.

Table 2.1 Descriptions of waves and durations.

Name	Descriptions	Duration
P wave	Represents theatrial depolarization.	Shorter than 0.12 seconds
PR interval	The interval between the points of the P wave to Q wave.	Longer than 0.12 seconds and shorter than 0.2 seconds.
QRS complex	Represents the ventricular depolarization and atrial repolarization.	Longer than 0.08 seconds and shorter than 0.12 seconds.
ST segment	The period during which the ventricles are depolarized.	Longer than 0.08 seconds and shorter than 0.12 seconds
T wave	The last wave of a normal cardiac cycle, representing the ventricular repolarization.	Shorter than 0.16 seconds
RR interval	The interval between two R waves.	Longer than 0.6 seconds and shorter than 1.2 seconds

While the heartbeats are caused by a series of electrical activities in the heart, we can collect and record these signals by attaching electrodes on the surface of the skin. When measuring ECG, usually more than two electrodes are used and they can be combined into a pair whose output is called a lead. The most common clinically-used one is 12-lead ECG where ten electrodes are used. Each electrode has a specific label (name), including RA, LA, RL, LL, V1, V2, V3, V4, V5, and V6. The placements and labels of electrodes are illustrated in Fig 2.2 and Table 2.2, respectively.

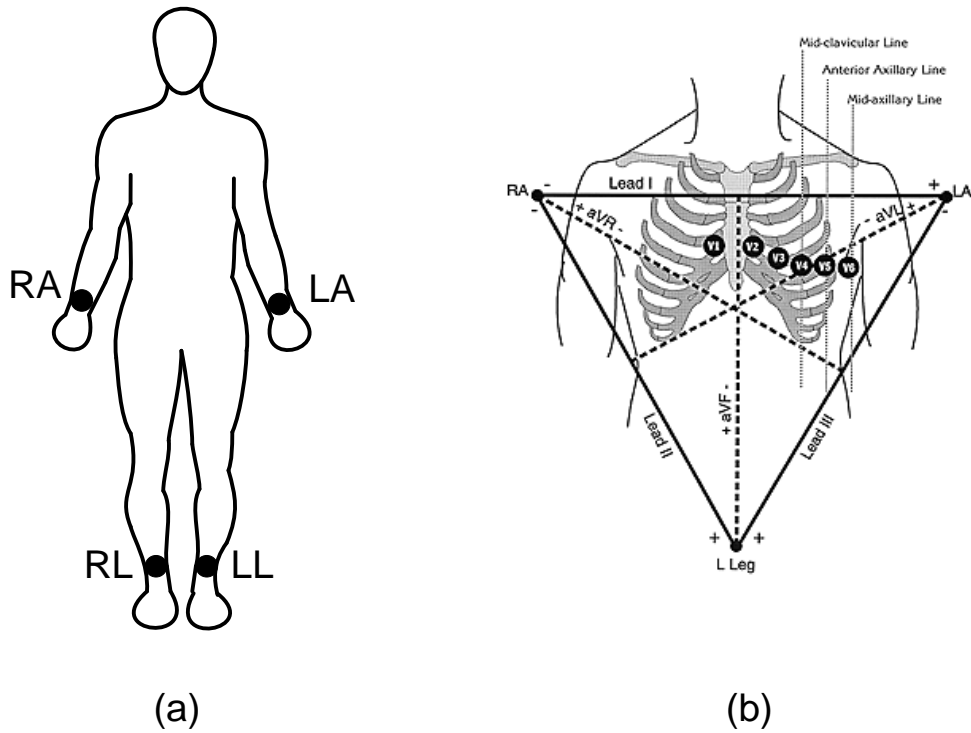


Figure 2.2 Placements of electrodes

Table 2.2 Placements of electrodes

Electrodes' label	Placement
RA	On the right arm.
LA	On the left arm.
RL	On the right leg.
LL	On the left leg.
V1	In the space, between rib 4 and rib 5, to the right side of the breastbone.
V2	In the space, between rib 4 and rib 5, to the left side of the breastbone.
V3	In the place between lead V2 and lead V4.
V4	In the space between rib 5 and rib 6, and on an imaginary line extended from the collarbone's midpoint.
V5	In the place between lead V4 and lead V6.
V6	In the space horizontally even with lead V4 and V5, and on an imaginary line extended from the middle of the armpit.

The twelve leads contain six precordial leads (V1~V6) in the horizontal plane, three standard limb leads (I, II, III), and three augmented limb leads (aVR, aVL, aVF) in the frontal plane. The twelve leads can also be divided into two types: bipolar and unipolar. While the former has one positive and one negative pole, the latter has two poles with the negative one made of signals from many other electrodes. For example, leads I, II, and III are bipolar leads, while others are unipolar leads. The definitions of twelve leads are given as below.

1. Lead aVR: the positive electrode is on the right arm and the negative one is a combination of two electrodes on the left arm and left leg.

$$\text{Lead aVR} = V_{RA} - (V_{LA} + V_{LL}) / 2 \quad (2.1)$$

2. Lead aVL: the positive electrode is on the left arm and the negative one is a combination of two electrodes on the right arm and left leg.

$$\text{Lead aVL} = V_{LA} - (V_{RA} + V_{LL}) / 2 \quad (2.2)$$

3. Lead aVF: the positive electrode is on the left leg and the negative one is a combination of two electrodes on the left arm and right arm.

$$\text{Lead aVF} = V_{LL} - (V_{LA} + V_{RA}) / 2 \quad (2.3)$$

4. Lead I: the positive electrode is on the left arm and the negative one is on the right arm.

$$\text{Lead I} = (V_{LA} - V_{RA}) \quad (2.4)$$

5. Lead II: the positive electrode is on the left leg and the negative one is on the right arm.

$$\text{Lead II} = (V_{LL} - V_{RA}) \quad (2.5)$$

6. Lead III: the positive electrode is on the left leg and the negative one is on the left arm.

$$\text{Lead III} = (V_{LL} - V_{LA}) \quad (2.6)$$

Of the 12 leads in total, each records the electrical activity of the heart from a different perspective, which also correlates to different anatomical areas of the heart for the purpose of identifying acute coronary ischemia or injury. Two leads that look at neighbouring anatomical areas of the heart are said to be contiguous. The relevance of this is in determining whether an abnormality on the ECG is likely to represent true disease or a spurious finding.

Modern ECG monitors offer multiple filters for signal processing. The most common settings are monitor mode and diagnostic mode. In monitor mode, the low-frequency filter is set at either 0.5Hz or 1Hz and the high-frequency filter is set at 40Hz. This limits artifacts for routine cardiac rhythm monitoring. The high-pass filter helps reduce wandering baseline and the low-pass filter helps reduce 50- or 60-Hz power line noise.

2.2 MIT-BIHECGdatabase

The MIT-BIH Arrhythmia Database was the first generally available set of standard test material for evaluation of arrhythmia detectors, and it has been used for that purpose as well as for basic research into cardiac dynamics at about 500 sites worldwide since 1980. Together with the American Heart Association (AHA) Database, it played an interesting role for evaluating automated arrhythmia analysis in research community. The ECG recordings came from the Beth Israel Deaconess Medical Center and were further digitized and annotated by a group at Massachusetts Institute of Technology. The database contains a total of 48 half-hour data, two-channel, 24-hour, obtained from 47 subjects. The subjects included 25 men aged 32 to 89 years and 22 women aged 23 to 89 years; approximately 60% of the subjects were inpatients. One channel is a modified limb II (MLII), and the other is usually V1 but can be V2, V4, or V5. The sample rate is 360Hz and each sample point is scalar quantized into 11 bits.

Most MIT-BIH databases include one or more sets of annotations for each recording. Annotations are labels that point to specific locations within a recording and describe events

at those locations. The annotators were instructed to use all evidence available from both signals to identify every detectable QRS complex. For example, many of the recordings that contain ECG signals have annotations that indicate the times of occurrence and types of each individual heart beat. The standard set of annotation codes was originally defined for ECGs, and includes both beat annotations and non-beat annotations. Most MIT-BIH databases use these codes(annotation) as described below.

Table 2.3 Beat annotations:

Code	Description
N	Normal beat (displayed as ".•")
L	Left bundle branch block beat
R	Right bundle branch block beat
B	Bundle branch block beat (unspecified)
A	Atrial premature beat
a	Aberrated atrial premature beat
J	Nodal (junctional) premature beat
S	Supraventricular premature or ectopic beat (atrial or nodal)
V	Premature ventricular contraction
r	R-on-T premature ventricular contraction
F	Fusion of ventricular and normal beat
e	Atrial escape beat
j	Nodal (junctional) escape beat
n	Supraventricular escape beat (atrial or nodal)
E	Ventricular escape beat
/	Paced beat
f	Fusion of paced and normal beat
Q	Unclassifiable beat
?	Beat not classified during learning

Table 2.4 Non-beat annotations:

Code	Description
[Start of ventricular flutter/fibrillation
!	Ventricular flutter wave
]	End of ventricular flutter/fibrillation
x	Non-conducted P-wave (blocked APC)
(Waveform onset
)	Waveform end
p	Peak of P-wave
t	Peak of T-wave
u	Peak of U-wave
`	PQ junction
'	J-point
^	(Non-captured) pacemaker artifact
	Isolated QRS-like artifact
~	Change in signal quality
+	Rhythm change
s	ST segment change
T	T-wave change
*	Systole
D	Diastole
=	Measurement annotation
“	Comment annotation
@	Link to external data

As shown in Fig 2.3, “A” and “.” represent atrial premature beat and normal beats and can be seen in MIT-100.

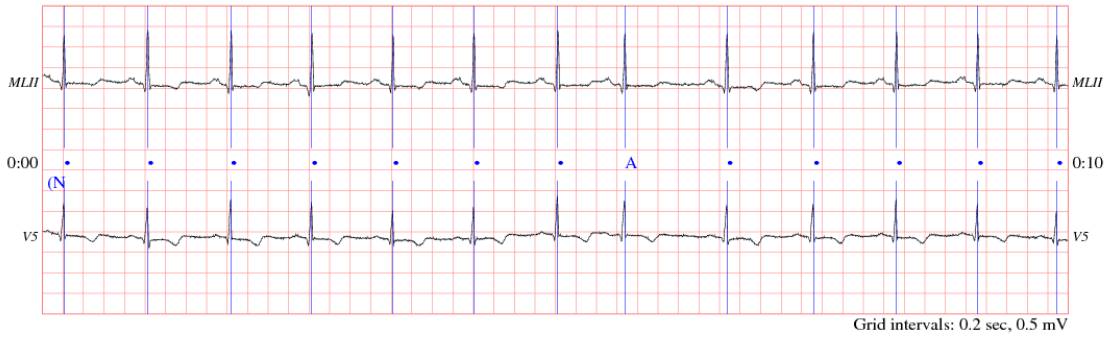


Figure 2.3 MIT-100 waveform

As shown in Fig 2.4 – Fig 2.6, several annotations are combined in MIT 205 with “F” and “V”, or with only specific annotation such as “L” in MIT-207 and “R” in MIT-118.

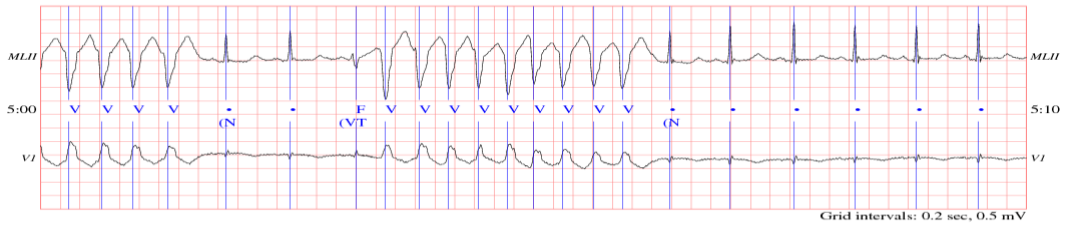


Figure 2.4 MIT-205 waveform

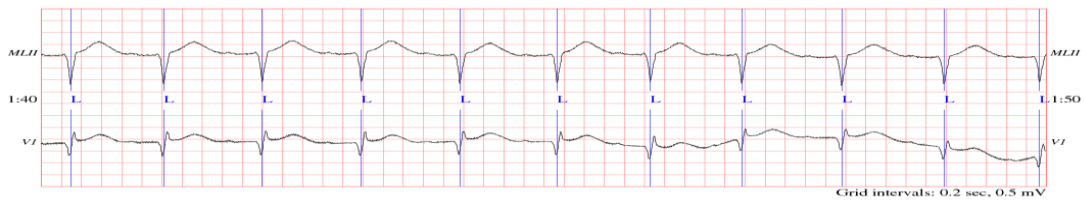


Figure 2.5 MIT-207 waveform



Figure 2.6 MIT-118

Chapter 3 Hilbert-Huang Transform for ECG Denoising

ECG signals are very weak compared to the measurement noise, so that some analysis tools are needed for signal denoising. Hilbert-Huang Transform (HHT) has become a powerful tool for signal analysis, since its introduction in 1996. This is due to its ability to extract periodic components which are embedded in a certain signal. This chapter briefly introduces HHT and its applications to ECG signal denoising, especially on high frequencies denoising.

3.1 Hilbert-Huang Transform

Traditional data analysis methods are derived by assuming that the signals are linear and stationary. In recent years some new methods have been proposed which apply an adaptive basis to analyze nonstationary and nonlinear data. Among them, HHT seems to be a good approach which matches all the requirements.

The HHT consists of two parts: empirical mode decomposition (EMD) followed by Hilbert spectral analysis (HAS). For nonlinear and nonstationary data, this method provides a powerful analysis, especially for time-frequency analysis and energy representations. In addition, the HHT displays the physical meanings of signals under investigation. The power of the method is verified by experiment and its applications have been widely studied.

3.1.1 Empirical mode decomposition (EMD)

As discussed by Huang et al[20], EMD is the first step to deal with data from nonstationary and nonlinear processes. The decomposition is based on the simple assumption that any data is composed of different intrinsic modes functions (IMF). Each IMF, linear or nonlinear, represents a simple oscillation, which has the same number of extrema and zero-crossings. At any given time, the data may have many different coexisting modes of oscillation, one superimposing on the others. Each of these oscillatory modes IMF must meet

the following two conditions:

(1) In the whole data set, an IMF with the number of zero and extreme crossings must equal or differ at most by one

(2) At the random time, the mean value of two envelopes which are defined by the local maximum and local minimum need to be zero. On the time axis, this implies that the envelopes are symmetric.

With the definition of the IMF, we can observe that IMF is typical of an oscillatory mode. The IMF not only represents constant amplitude and frequency, as each harmonic component does, but also has a variable amplitude and frequency as functions of time.

The procedure of producing IMFs starts with finding local maximum and minimum of the signal. The up and down of the signal are calculated by cubic spline interpolation. The average value of the curve's maxima and minima is called m_1 with relation to $x(t)$ as:

$$x(t) - m_1(t) = h_1(t) \quad (3.1)$$

The first component h_1 is checked to see if it satisfies the above-mentioned two conditions. If not satisfied, we treat h_1 as original data and repeat the above process to obtain

$$h_1(t) - m_{11}(t) = h_{11}(t) \quad (3.2)$$

This calculation is repeated till we find out h_{1k} ,

$$h_{1(k-1)}(t) - m_{1k}(t) = h_{1k}(t) \quad (3.3)$$

which satisfies the two conditions and is designed as the first IMF $c_1(t) = h_{1k}(t)$. It means c_1 should contain the shortest periodic component of the signal.

After taking c_1 out of the original data, we have the residue,

$$x(t) - c_1(t) = R_1(t) \quad (3.4)$$

Since the residue still contains the long-cycle variations in the data, it will be treated as the

new data followed by the filtering process. This procedure is repeated with all R_i

$$R_1(t) - c_2(t) = R_2(t), \dots, R_{n-1}(t) - c_n(t) = R_n(t) \quad (3.5)$$

The process can be stopped when $R_n(t)$ becomes so small that no more IMFs can be extracted or when R_n becomes a single function. By summing up the IMFs, the $x(t)$ can be represented by:

$$x(t) = \sum_{i=1}^n c_i(t) + R_n(t) \quad (3.6)$$

By decomposing a data into n-empirical modes, the whole EMD can be considered as the mean trend or the scale processing with each IMF representing the characteristics of each scale. In other words, the IMF eliminates the nonstationary character of the original signal.

3.1.2 Hilbert Transform

Having obtained the IMF components, the Hilbert transform process is performed on every IMF to obtain a new time series $y_i(t)$ in the transform domain as follow

$$y_i(t) = \frac{1}{\pi} p \int \frac{c_i(t')}{t-t'} dt' \quad (3.7)$$

With this definition, a complex series $z_i(t)$ is formed in terms of

$$z_i(t) = c_i(t) + jy_i(t) = a_i(t)e_i^{j\theta(t)} \quad (3.8)$$

where the amplitude of $z_i(t)$ will be:

$$a_i(t) = \sqrt{c_i^2(t) + y_i^2(t)} \quad (3.9)$$

and phase

$$\theta_i(t) = \arctan\left(\frac{y_i(t)}{c_i(t)}\right) \quad (3.10)$$

In addition, instantaneous frequency is calculated by

$$\omega_i(t) = \left(\frac{d\theta_i(t)}{dt} \right) \quad (3.11)$$

Unlike the FFT, $a_i(t)$ and $\omega_i(t)$ derived by HHT are functions of time t , so the HHT can characterize the variation of power with time.

3.2 HHT-based denoising

After EMD on the noisy signal are conducted, the energy of the IMFs is analyzed to separate the IMF components into signal-dominated parts and noise-dominated parts. By exploiting the fact that the scale of the IMFs components is dramatically increasing, the energy of IMFs of Gaussian white noise will reduce as the number of decomposition increases. With this approach, the denoising processing based on HHT will be performed by applying filtering on each IMF.

A. Energy analysis

Following the work of [24-25] the energy of $x(t)$ can be represented as

$$E = \sum_{t=1}^T a^2(t) \quad (3.12)$$

According to the observation of N.E.Huang [20], when the energy approaches the lowest point, this point is considered as the boundary between the most noisy part and signal part. When the energy of IMF_i lower than IMF_{i+1} , IMF_i is considered to be the boundary.

B. Soft-threshold denoising process

Soft-threshold denoising method is proposed by Donoho et al. [21-23]. Each IMF component dominated by the Gaussian white noise must carry out soft-threshold denoising process, and the corresponding threshold is

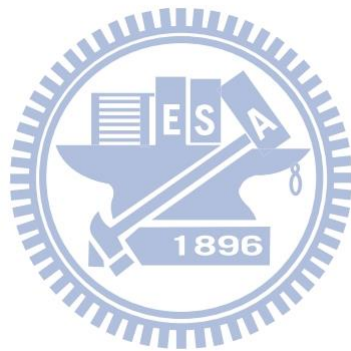
$$thr_i = \sigma_i \sqrt{2 \log(N)} \quad (3.13)$$

where N is the length of each IMF. σ_i^2 is the noise variance in each IMF and is calculated by

the equation $\sigma_i = MAD_i / 0.6745$. MAD_i is the absolute median deviation of the i -th layer IMF_i

$$MAD_i = \text{median}(\text{abs}(IMF_i - \text{median}(IMF_i))) \quad (3.14)$$

After all IMFs are applied with soft-threshold denoising process, we reconstruct the denoised signal by overlaying the EMD.



Chapter 4 VQ-based ECG Compression

Vector quantization (VQ) is a lossy data compression method based on the principle of block coding. It is a fixed-to-fixed length algorithm. In the earlier days, the design of a vector quantizer (VQ) is considered to be a challenging problem due to the need for multi-dimensional integration. In 1980, Linde, Buzo, and Gray (LBG) proposed a VQ codebook construction algorithm based on a training sequence, which bypasses the need for multi-dimensional integration.

4.1 Vector Quantization

Extensive studies of vector quantizers or multidimensional quantizers have long been performed by many researchers [1-5]. The design of optimal vector quantizers from empirical data were proposed by Linde, Buzo, and Gray [6] using a clustering approach. This algorithm is now commonly referred to as the LBG algorithm. A vector quantizer can be defined as a mapping Q of K -dimensional Euclidean space R^k into a finite subset Y of R^k . Thus,

$$Q: R^k \rightarrow Y \quad (4.1)$$

where $Y = (\hat{x}_i; i = 1, 2, \dots, N)$ is a set of N reproduction vectors. As shown in Fig 4.1, the VQ can also be seen as a combination of two functions: an encoder, which represents the input vector x with an index of the reproduction vector specified by $Q(x)$, and a decoder, which uses this index to generate the reproduction vector \hat{x}_i . The best mapping Q is the one which minimizes a distortion measure $d(x, \hat{x})$ which represents the penalty or cost associated with reproducing vectors x by \hat{x} . The LBG algorithm and other variations of this algorithm are derived based upon this minimization, using a training set as the signal.

One simple distortion measure for waveform coding is the square error distortion given by

$$d(x, \hat{x}) = \|x - \hat{x}\|^2 = \sum_{j=0}^{K-1} (x_j - \hat{x}_j)^2 \quad (4.2)$$

A weighted mean square error (WMSE) distortion can also be used [7]. Other error distortion measures have also been suggested, but they are too expensive computationally for practical implementation. One problem with vector quantization is that the encoder needs to search the whole codebook in order to identify the nearest vector template matching to an input vector.

The most important part which consumes the most time is VQ codebook design. The goal in designing an optimal vector quantizer is to obtain a codebook consisting of N reproduction vectors, such that it minimizes the expected distortion. Optimality is said to be achieved if there is no other quantizer that can achieve the minimum expected distortion. Lloyd [8] proposed an iterative nonvariational technique known as his "Method I" for the design of scalar quantizers. Linde et al [9]. extended Lloyd's basic approach to the general case of vector quantizers.

Let the expected distortion be approximated by the time-averaged square error distortion given by

$$D(x, q(x)) = \frac{1}{N} \sum_{i=0}^{N-1} d(x_i, \hat{x}_i) \quad (4.3)$$

The LBG algorithm for an unknown distribution training sequence is given as follows

1) Let N = number of levels; distortion threshold $\varepsilon \geq 0$. Assume an initial N level reproduction alphabet \hat{A}_0 , and a training sequence $(x_j; j = 0, 1, \dots, n-1)$, and m = number of iterations, set to zero.

2) Given $\hat{A}_m = (y_i; i = 1, \dots, N)$, find the minimum distortion partition $P(\hat{A}_m) = (S_i; i = 1, \dots, N)$ of the training sequence: $x_j \in S_i$, if $d(x_j, y_i) \leq d(x_j, y_l)$, for all

l. Compute the average distortion

$$D_m = D\left[\left(\hat{A}_m, P\left(\hat{A}_m\right)\right)\right] = (n-1) \sum_{j=0}^{n-1} \min_{y \in \hat{A}_m} d\left(x_j, y\right) \quad (4.4)$$

3) If $(D_{m-1} - D_m) / D_m \leq \varepsilon$, stop the iteration and use \hat{A}_m as the final reproduction alphabet; otherwise continue.

4) Find the optimal reproduction alphabet $\hat{x}\left(P\left(\hat{A}_m\right)\right) = \left(\hat{x}\left(S_i\right); i = 1, \dots, N\right)$ for $P\left(\hat{A}_m\right)$

where

$$\hat{x}\left(S_i\right) = \frac{1}{\left\|S_i\right\|} \sum_{j: x_j \in S_i} x_j \quad (4.5)$$

5) Set $\hat{A}_{m+1} = \hat{x}\left(S_i\right)$ increment m to $m+1$, and go to step 2).

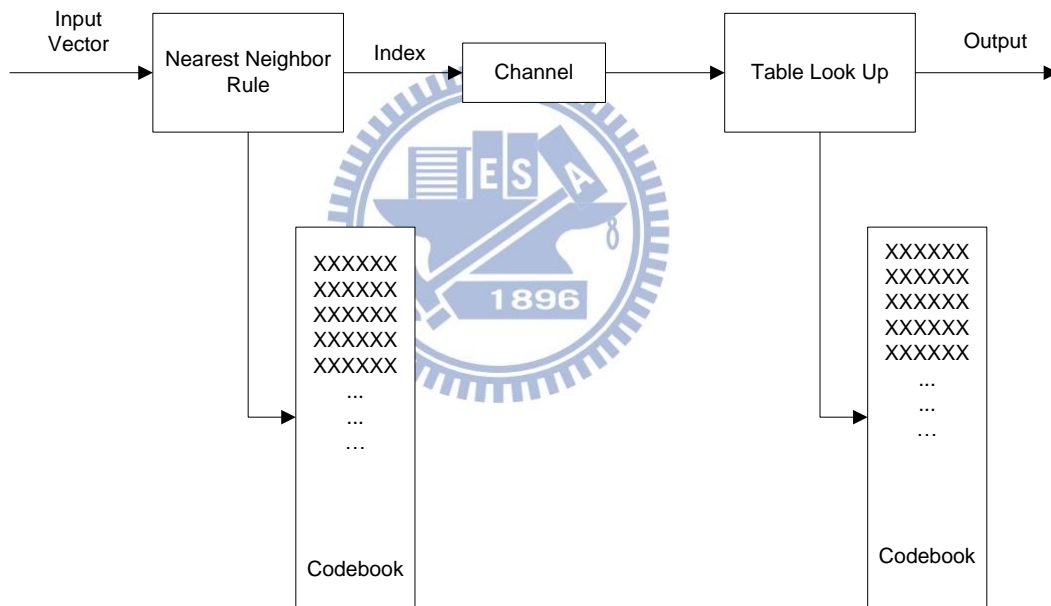


Figure 4.1 The VQ transmission system

In the above iterative algorithm an initial reproduction alphabet \hat{A}_0 was assumed in order to start the algorithm. There are a number of techniques to construct the initial codebook. The simplest technique is to use the first widely spaced words from the training sequence. Linde et al. [9] used a splitting technique where the centroid for the training sequence was calculated and split into two close vectors. The centroids or the reproduction vectors for the two partitions were then calculated. Each resulting vector was then split into two vectors

and the above procedure was repeated until an N -level initial reproduction vector was created. Splitting was performed by adding a fixed perturbation vector ε to each vector y_j producing two vectors $y_j + \varepsilon$ and $y_j - \varepsilon$.

4.2 VQ for ECG Compression

The lengths of heart-beat segments are different so each ECG cycle has to be normalized to a fixed length. A predefined length is obtained by calculating the average length of a large training set of ECG cycles. Cubic spline interpolation is then used due to the simplicity of construction, and accuracy of evaluation. The block diagram of VQ-based ECG compression is shown in Fig 4.2.

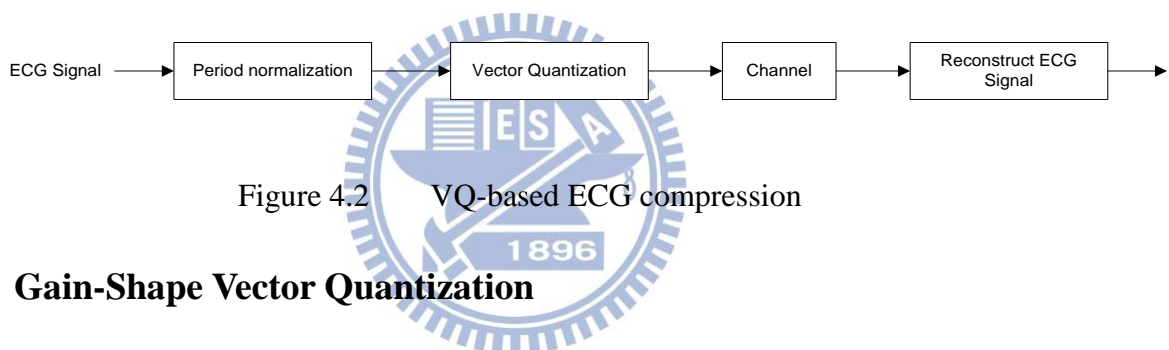


Figure 4.2 VQ-based ECG compression

4.2.1 Gain-Shape Vector Quantization

Although conventional VQ works well for its high compression ratio and high quality reconstruction, there exist many variants for different applications. The conventional VQ encoder requires computational complexity proportional to $k2^M$, which implies that its complexity grows exponentially. A large codebook is needed to achieve reasonable performance if the dynamic range of the input vector is large, since there should be more codewords to represent original input vectors. Therefore a good performance of VQ is reached at the cost of high encoding complexity due to the use of a large codebook. To solve this problem, gain-shape VQ (GSVQ) is used in this thesis. GSVQ is a technique that decomposes reproduction vector into a scalar gain and a shape vector, which is normalized by the root mean-square value of the vector components. This quantity is called the gain and

serves as a normalizing scale factor. The normalized input vector is called the shape. The basic idea of GSVQ is that the same pattern of variation in a vector may recur with a wide variety of gain values. It suggests that the probability distribution of the shape is approximately independent of the gain. We would then expect very little compromise in optimality with a product code structure. Viewing from another perspective, we can say that the code is permitted to handle the dynamic range of the vector separately from the shape of the vector. GSVQ was introduced in [10] and optimized in [11].

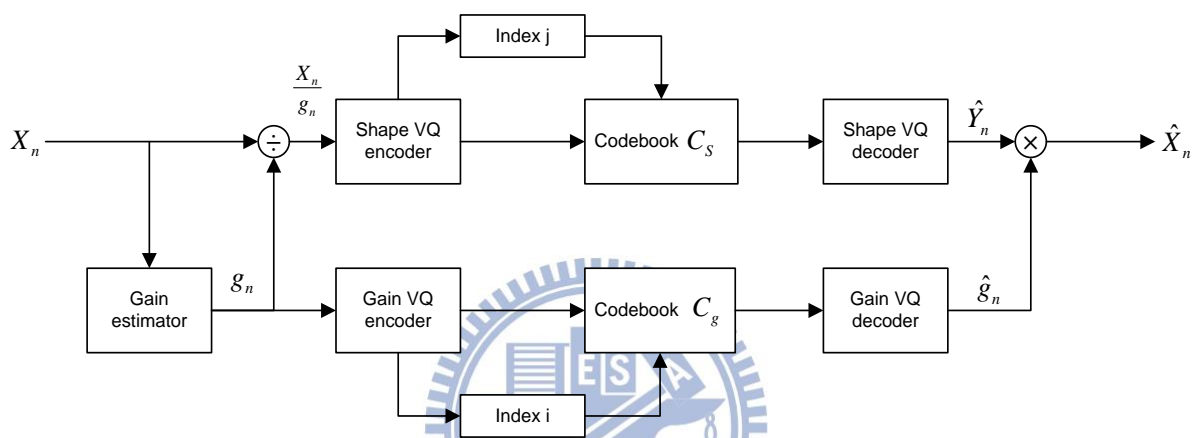


Figure 4.3 The gain-shape VQ system

In Gain-shape VQ, the gain g_n is the norm of a k -dimensional input vector X_n ,

$$g_n = \|X_n\| = \left(\sum_{i=1}^k x_{ni}^2 \right)^{1/2} \quad (4.6)$$

and shape S_n refers to the normalized input vector, that is,

$$S_n = X_n / g_n \quad (4.7)$$

All the shape vectors in the shape codebook C_s have unit gain. With this product code decomposition, the shape vector lies on the surface of a hypersphere in k -dimensional space and is therefore easier to quantize than the original vector X . In order to determine the optimal encoding structure, we begin by examining the performance criteria. Here we assume the squared error distortion measure

$$d(X, \hat{g}\hat{S}) = \|X - \hat{g}\hat{S}\|^2 \quad (4.8)$$

where \hat{g} is the quantized version of g and \hat{S} is the quantized version of the shape S . The gain and shape codebooks are denoted by C_g and C_s with sizes N_g and N_s , respectively. Expanding this expression gives

$$d(X, \hat{g}\hat{S}) = \|X\|^2 + \hat{g}^2 - 2\hat{g}(X'\hat{S}) \quad (4.9)$$

This distortion can be minimized over \hat{g} and \hat{S} in two steps. First select the shape vector S which minimizes the third term, that is, pick the \hat{S} that maximizes $X'\hat{S}$. Note that \hat{g} is always positive and its value does not influence the choice of \hat{S} . It is also important to note that the input vector need not be itself gain normalized in order to choose the best shape vector. Such normalization would involve division by the input gain and would significantly increase the encoder complexity. The maximum correlation selection obviates any such computation. Once the shape codeword is chosen, select the \hat{g} to minimize the resulting function of \hat{g} , thus

$$\|X\|^2 + \hat{g}^2 - 2\hat{g}(X'\hat{S}) = \|X\|^2 + (\hat{g} - (X'\hat{S}))^2 - \hat{g}(X'\hat{S})^2 \quad (4.10)$$

which is accomplished by choosing \hat{g} to minimize

$$[\hat{g} - X'\hat{S}]^2 \quad (4.11)$$

for the previously chosen (unit norm) S . Note that the second step requires only a standard scalar quantization operation, where the gain nearest to the quantity $X'\hat{S}$ is selected from the gain codebook.

The optimal encoding rule is a two-step procedure, where the first step involves a single feature (the shape) and one codebook. The second step depends on the first step in its computation of the nearest neighbor for the second feature (the gain) in its codebook. In

effect, the first step affects the distortion measure used to compute the second step. Note that this is the reverse of the mean-removed VQ where the scalar parameter is quantized followed by the residual (corresponding to the shape) quantized. This procedure can also be seen to yield the optimal (nearest neighbor) product codeword by observing that

$$\min_{\hat{S}, \hat{g}} \left(\hat{g}^2 - 2\hat{g} \left(X' \hat{S} \right) \right) = \min_{\hat{g}} \left(\hat{g}^2 - 2\hat{g} \max_{\hat{S}} \left(X' \hat{S} \right) \right) \quad (4.12)$$

Both the encoder and decoder of the gain-shape quantizer are shown in Fig 4.4 and 4.5

We next consider the task of codebook design for gain-shape VQ. We begin with a training set T of input vectors, x_i , each of which realizes the random vector X . The objective is to find the shape and gain codebooks that minimize the average distortion incurred in encoding the training vectors. There are several variations of the Lloyd algorithm by which this task can be accomplished [11], but we focus on the basic one with good properties.

A Gain-shape VQ is completely described by three objects:

- The gain codebook $C_g = \{ \hat{g}_i; i = 1, 2, \dots, N_g \}$,
- The shape codebook $C_s = \{ \hat{S}_j; j = 1, 2, \dots, N_s \}$, and
- A partition $R = \{ R_{i,j}; i = 1, 2, \dots, N_g; j = 1, 2, \dots, N_s \}$ of $N_g \times N_s$ cells describing the encoder, that is, if $x \in R_{i,j}$, then x is mapped into (i,j) and the resulting reproduction is formed from the shape-gain vector (\hat{g}_i, \hat{S}_j) . We express this as $g(x) = \hat{g}_i$ and $S(x) = \hat{S}_j$.

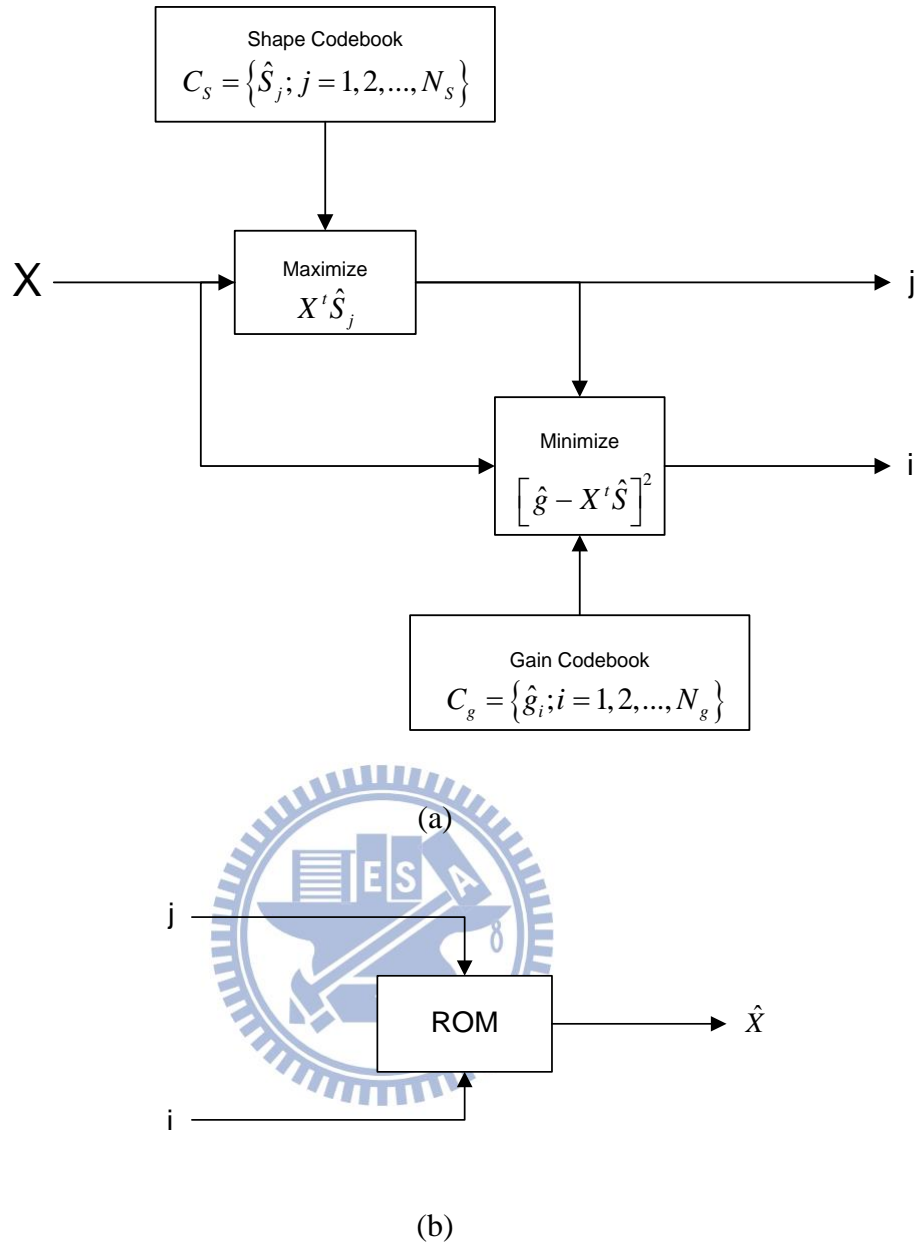


Figure 4.4 Gain-shape VQ (a) encoder (b)decoder

4.2.2 Multistage VQ

In some cases, ECG signals have a wide variation of gain or of mean values, then shape-gain or mean-removed VQ methods are not likely to be very helpful. This motivates own research into ECG compression using other variants of VQ. If the dimension is quite large, partitioned VQ would certainly solve the complexity problem but might severely degrade performance when there is substantial statistical interdependence between different subvectors. If we are concerned with storage as well as search complexity, then tree-

structured VQ and classified VQ are not helpful. Furthermore, transform VQ may be of limited use if the degree of achievable compaction still results in a high vector dimension.

One alternative technique that has proved valuable in speech and image coding applications is the multistage or cascaded VQ [12]. The basic idea of multistage VQ (MSVQ) is to divide the encoding task into successive stages, where the first stage performs a coarse quantization of the input vector using a small codebook. Then, a second stage quantizer operates on the error vector between the original and first stage quantizer's output. The quantized error vector provides a second approximation to the original input vector, thereby leading to a refined representation of the input. We first consider the special case of two-stage VQ as illustrated in Fig 4.5. The input vector X is quantized by first stage vector quantizer denoted by Q_1 . The quantized approximation \hat{X}_1 is then subtracted from X to produce the error vector E_2 . This error vector is then applied to a second vector quantizer Q_2 , yielding the quantized output \hat{E}_2 . The overall approximation \hat{X} to the input X is formed by summing the first and second approximations, \hat{X}_1 and \hat{E}_2 . The encoder for this MSVQ scheme transmits a pair of indexes specifying the selected code vectors for each stage. The decoder performs two table lookups and then sums the two code vectors.

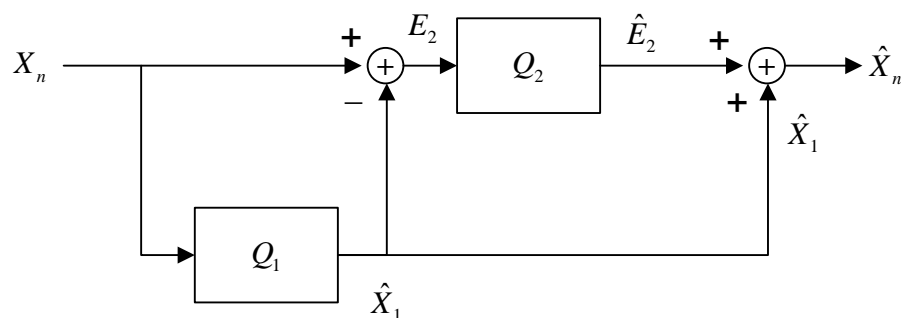


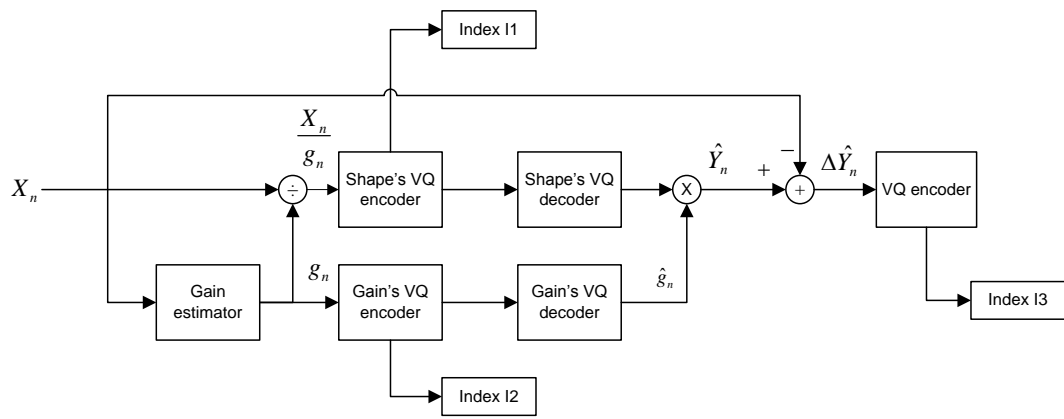
Figure 4.5 The Two-Stage MSVQ system

By inspection of the figure it may be seen that the input-output error is equal to the quantization error introduced by the second stage, $X - \hat{X} = E_2 - \hat{E}_2$. From this equation it

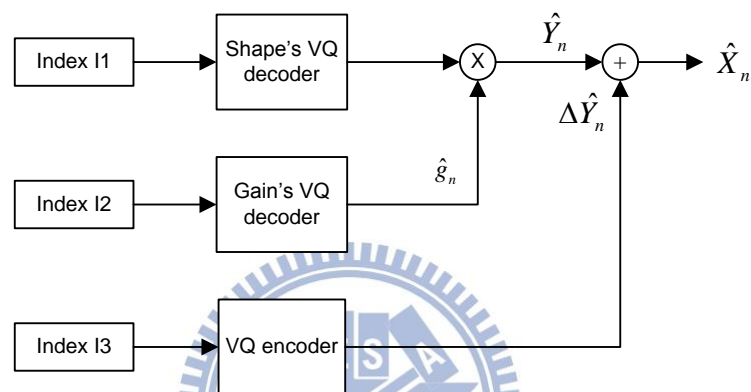
can be readily seen that the signal to quantizing noise power ratio in dB (SNR) for the two stage quantizer is given by $SNR = SNR_1 + SNR_2$, where SNR_i is the SNR for the i -th quantizer. In comparison with a single quantizer with the same total number of bits, a two-stage quantizer has the advantage that the codebook size of each stage is considerably reduced so that both the storage requirement and the search complexity are substantially lowered. The price paid for this advantage is an inevitable reduction in the overall SNR achieved with two stages. The general MSVQ method can be generalized by induction from the two-stage scheme. By replacing the box labeled Q_2 in Fig 4.5, with a two-stage VQ structure, we obtain 3-stage VQ. By replacing the last stage of an m -stage structure, we increase the number of stages to $m + 1$.

An ECG compression technique is suggested in this thesis that takes into consideration both dynamic range of the input vector, as well as light complexity of the reconstruction. In practice, multistage coders often have only two and occasionally three stages. As far as we know, there has been no report of a coding system using four or more stages. In our work, the dynamic range is reduced by using Gain-shape VQ as the first stage. The second stage quantizer is then used to quantize the first stage error vector to provide a further refinement as shown in Fig 4.6. The encoder transmits indexes I_1, I_2, I_3 to the decoder, which then performs

a table-lookup in the respective codebooks and forms the multiply and sum as Fig 3.8. The complexity is reduced from $N = \prod_{i=1}^m N_i \rightarrow \sum_{i=1}^m N_i$. Thus both the complexity and storage requirements can be greatly reduced using multistage GSVQ.



(a)



(b)

Figure 4.6 The proposed ECG compression system: (a) the encoder, (b) the decoder

Chapter 5 **JPEG2000-Based ECG Compression**

With the increasing use of multimedia technologies, image compression requires higher performance as well as new features. To address this need in the specific area of still image encoding, a new standard the JPEG2000 is currently being developed. It is not only intended to provide rate-distortion and subjective image quality performance superior to existing standards, but also to provide features and functionalities that current standards can either not address efficiently or in many cases cannot address at all. Lossless and lossy compression, embedded lossy to lossless coding, progressive transmission by pixel accuracy and by resolution, robustness to the presence of bit-errors and region-of-interest coding, are some representative features. It is interesting to note that JPEG2000 is being designed to address the requirements of a diversity of applications, e.g. Internet, color facsimile, printing, scanning, digital photography, remote sensing, mobile applications, medical imagery, digital library and E-commerce. This chapter presents a brief introduction to JPEG2000, including JPEG compressing architecture and its application to ECG signals.

5.1 JPEG2000

Since the mid-80s, members from both the International Telecommunication Union (ITU) and the International Organization for Standardization (ISO) have been working together to establish a joint international standard for the compression of grayscale and color still images. This effort has been known as JPEG, the Joint Photographic Experts Group the “joint” in JPEG refers to the collaboration between ITU and ISO.

The JPEG2000 standard provides a set of features that are of importance to many high-end and emerging applications. Its applications include Internet, color facsimile, printing, scanning (consumer and prepress), digital photography, remote sensing, mobile, medical imagery, digital libraries/archives and Ecommerce. Each application area imposes some requirements that the standard should fulfill. Some of the most important features that this

standard should possess are the following:

- Superior low bit-rate performance
- Lossless and lossy compression
- Progressive transmission by pixel accuracy and resolution
- Region-of-Interest Coding
- Random codestream access and processing
- Robustness to bit-errors
- Open architecture
- Content-based description
- Side channel spatial information (transparency)
- Protective image security
- Continuous-tone and bi-level compression

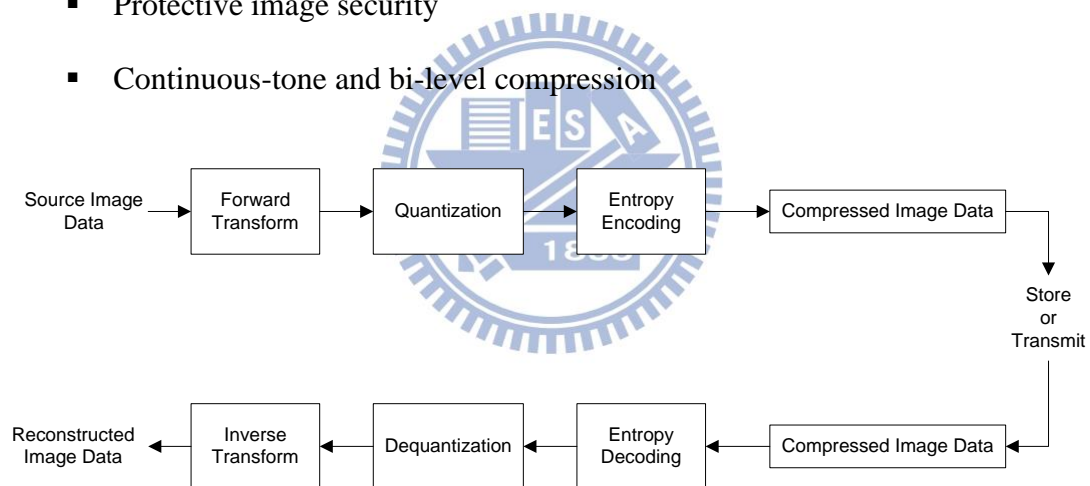


Figure 5.1 The block diagrams of JPEG2000 codec

The block diagram of the JPEG2000 codec is illustrated in Fig. 5.1. The discrete transform is first applied on the source image data. The transform coefficients are then quantized and entropy coded, before forming the output codestream (bitstream). The decoder is the reverse of the encoder. The codestream is first entropy decoded, dequantized and inverse discrete transformed, thus resulting in the reconstructed image data.

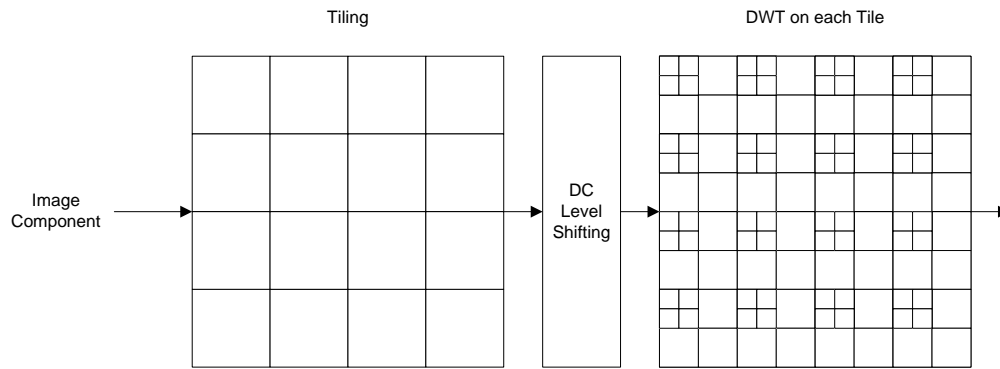


Figure 5.2 Tiling, DC level shifting and DWT of each image tile component

The processing method of JPEG2000 is based on the standard of image tiles, 'Tiling'. The term 'tiling' refers to the partition of the original (source) image into rectangular nonoverlapping blocks (tiles), which are compressed independently, as though they were entirely distinct images. All operations, including component mixing, wavelet transform, quantization and entropy coding are performed independently on the image tiles. Tiling reduces memory requirements and since they are also reconstructed independently, they can be used for decoding specific parts of the image instead of the whole image. All tiles have exactly the same dimensions, except maybe those at the right and lower boundary of the image. Arbitrary tile sizes are allowed, up to and including the entire image (i.e. the whole image is regarded as one tile). Components with different sub-sampling factors are tiled with respect to a high-resolution grid, which ensures spatial consistency on the resulting tile components. As the overview of JPEG2000 encoding and decoding mentioned above, the most important component of the standard is the specification of bitstream syntax, which is addressed comprehensively in the standard documentation. The core structure of the JPEG2000 encoder which is considered under the flow-of-bit view can be presented as a typical sequence as below

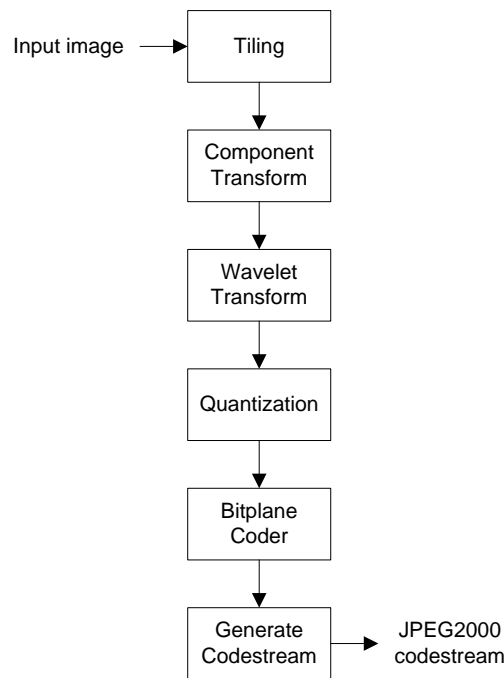


Figure 5.3 flow-of-bit viewof JPEG2000 encoder

- The input image is decomposed into components.
- The image and its components are divided into non-overlapping rectangular tiles.
- The wavelet transform is applied on individual tile. Each tile is decomposed in different resolution levels.
- These decomposition levels are decided by the coefficients that describe the frequency characteristics of local areas of the *tile-component*.
- The subbands of coefficients are quantized and formed into arrays of “code-blocks”.
- The bit-planes of the coefficients in a “code-block” are entropy coded.
- Markers are added in the bitstream to allow error reconstruct.

It should be noted here that the basic encoding engineof JPEG2000 is based on EBCOT (Embedded BlockCoding with Optimized Truncation of the embeddedbitstreams) algorithm, which is described in more details in[15-16].

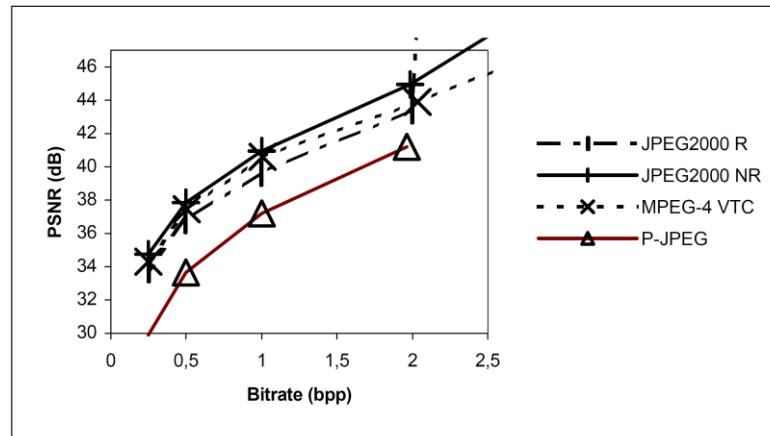


Figure 5.4 Results obtained by progressive JPEG (P-JPEG), progressive JPEG2000 (both embedded lossless, R, and lossy, NR, versions) and MPEG-4 VTC baseline.[17]

Fig5.4 depicts the rate-distortion behavior obtained by applying various progressive compression schemes on a natural image. It is clearly seen that progressive lossy JPEG2000 outperforms all other schemes, including the non-progressive (i.e. baseline) variant of MPEG-4 visual texture coding (VTC), although the difference is not significant. The progressive lossless JPEG2000 does not perform as well as the former two, mainly due to the use of the reversible wavelet filters. However, a lossless version of the image remains available after compression, which can be of significant value to many applications (archiving, medical, etc.). As for the progressive JPEG, it is outperformed by far by all other algorithms, as expected for a relatively old standard.

5.2 JPEG2000 for ECG compression

The dependencies in ECG signals can be broadly classified into two types: The dependencies in a single ECG cycle and the dependencies across ECG cycles. These dependencies are sometimes referred to as intrabeat and interbeat dependencies, respectively. An efficient compression scheme needs to exploit both dependencies to achieve maximum data compression.

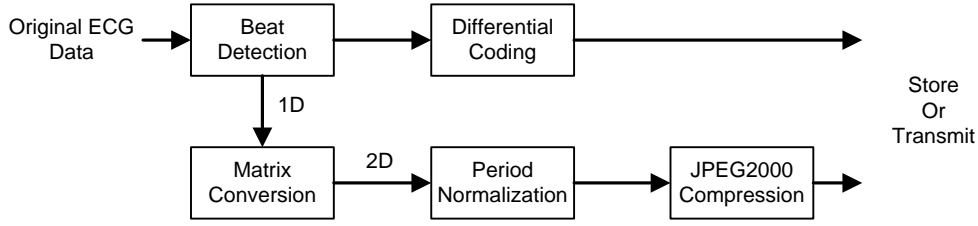


Figure 5.5 Block diagram of ECG encoder using JPEG2000

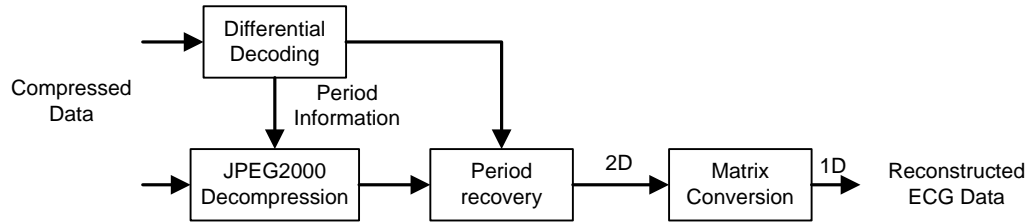


Figure 5.6 Block diagram of aECG decoder using JPEG2000

The block diagram of the proposed method is presented in Fig5.5 and 5.6. To compress the ECG data through a JPEG2000 codec, the one-dimensional ECG sequence needs to be processed to produce a two-dimensional matrix. Since it is desirable to exploit both the intrabeat and interbeat dependencies, the segmentation of the ECG sequence should be performed in such a fashion that the resulting matrix allows exploitation of both types of dependencies by the JPEG2000 codec. Thus, the first step in the proposed algorithm is to separate each “period” of the ECG as illustrated in Fig5.7. Each such period is then stored as one row of a matrix. It can be seen that the intrabeat dependencies are in the horizontal direction of the matrix and the interbeat dependencies are in the vertical direction. A matrix created using this approach is shown in Fig5.8 and Fig 5.9. Since each ECG period can have a different duration, the matrix generated using the above approach will have a different number of data points in each row. In order to exploit the interbeat dependencies using JPEG2000, we normalize each ECG period to the same length. Let $x_m = [x_m(1) \ x_m(2) \ \dots \ x_m(N_m)]$ denote the m-th ECG cycle. Then the period-normalized

ECG cycle $y_m = [y_m(1) \ y_m(2) \ \dots \ y_m(N_m)]$ is computed by using $\tilde{x}_m(t')$ is an interpolated version of the samples, $x_m(n)$, and

$$t' = \frac{(n-1)(N_m-1)}{(N-1)} + 1 \quad (4.1)$$

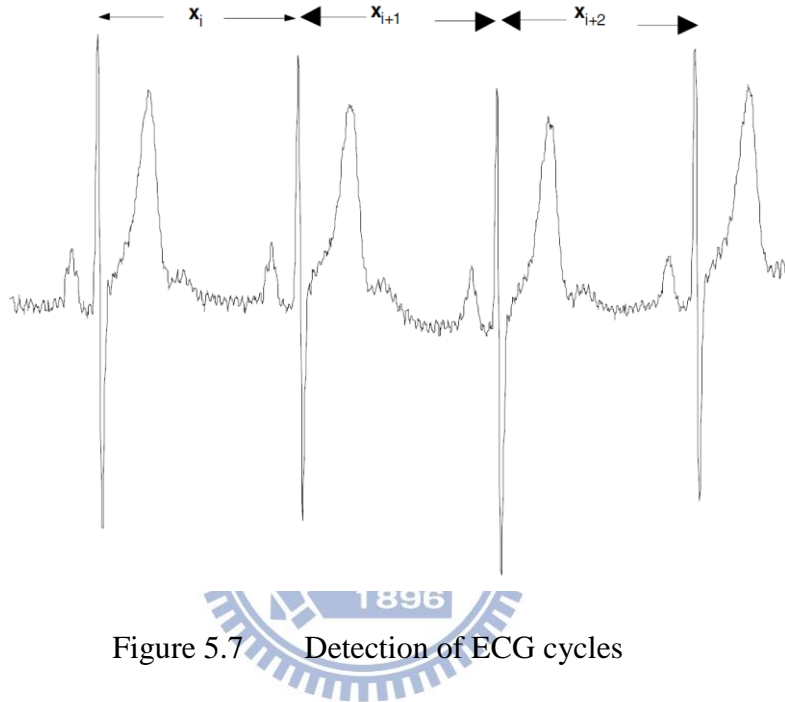


Figure 5.7 Detection of ECG cycles

where N_m is the period of the m -th ECG cycle, and N is the normalized period. We utilize cubic-spline interpolation to determine $\tilde{x}_m(t')$. The period-normalized matrix corresponding to the data in Fig5.8 is shown in Fig5.9.

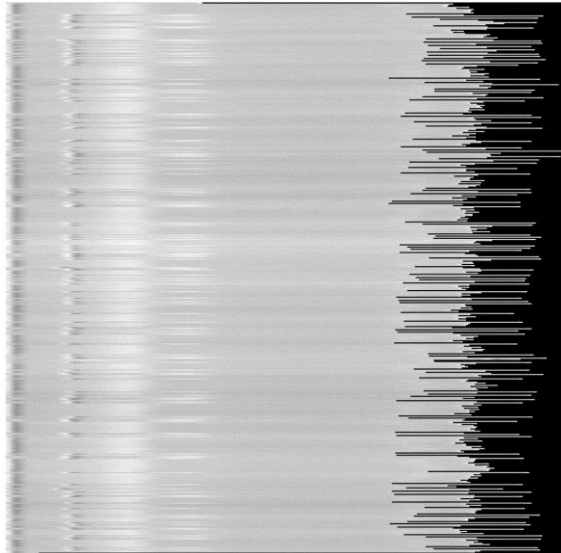


Figure 5.8 Before period normalization

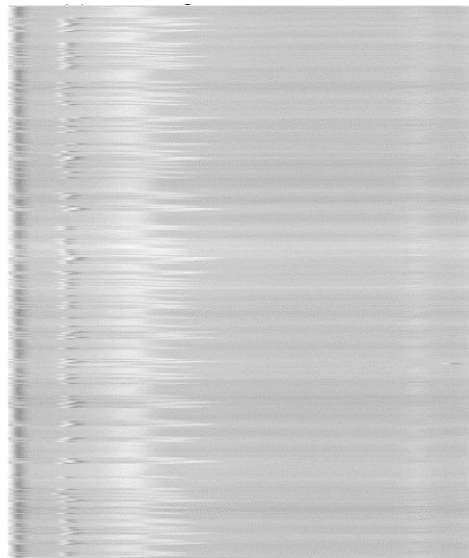


Figure 5.9 After period normalization

Besides compression efficiency, the proposed method benefits from desirable characteristics of the JPEG2000 codec, such as precise rate control and progressive quality. Note that the original periods ($N_m, m=1,2,K$) must be stored and sent to the decoder as side information. Once the decoder recovers the period-normalized ECG cycles, the original ECG cycles can be used to reconstruct ECG signal.

Chapter 6 Experimental Results

In the previous chapters we have described two new ECG compression algorithms. In this chapter, simulations are conducted to verify the proposed ECG compression algorithm. QRS complex detection and period normalization are applied for preprocessing. Algorithm I refers to the combined use of MSVQ and GSVQ. Algorithm II represents the ECG compression based on JPEG2000. Also included is the application of HHT to ECG signal denoising. In these algorithms, several MIT-BIH recordings are used as our ECG sources, and each is sampled at 360 sample/second and quantized with 11 bits. They are used for ECG compression as well as for signal denoising.

6.1 Preprocessing Data

Two preprocesses are applied to a dataset including MIT-100, MIT-108, MIT-119, MIT-122. We first have QRS detected for records MIT-100, MIT-119, MIT-122, and then perform period normalization to make each cycle of length 288 points. These period-normalized signals are used as ECG sources for Algorithm I and Algorithm II. MIT-108 is used as the source for the HHT-based signal denoising. For ECG compression experiments, we choose the first 1,500 ECG cycles as training sequences, and the latter 200 ECG cycles as testing sequences.

Percent root mean square difference (PRD) and compression ratio (CR) are used to evaluate the performance. PRD is a measure of the fidelity of the compressed signal and is given by

$$PRD(\%) = \sqrt{\frac{\sum_{i=1}^N [x(i) - \hat{x}(i)]^2}{\sum_{i=1}^N x(i)^2}} \times 100 \quad (6.1)$$

where L is the number of ECG samples, x is the original signal, and \hat{x} is the reconstructed signal. The CR is defined as

$$CR = \frac{n_x}{n_s + n_g + n_d} \quad (6.2)$$

where n_x denotes the number of bits per sample in the original signal, n_s denotes the number of bits per sample to code the index of shape, n_g denotes the number of bits per sample used to code the index of gain, and n_d denotes the number of bits per sample used to code the difference signal of the second stage.

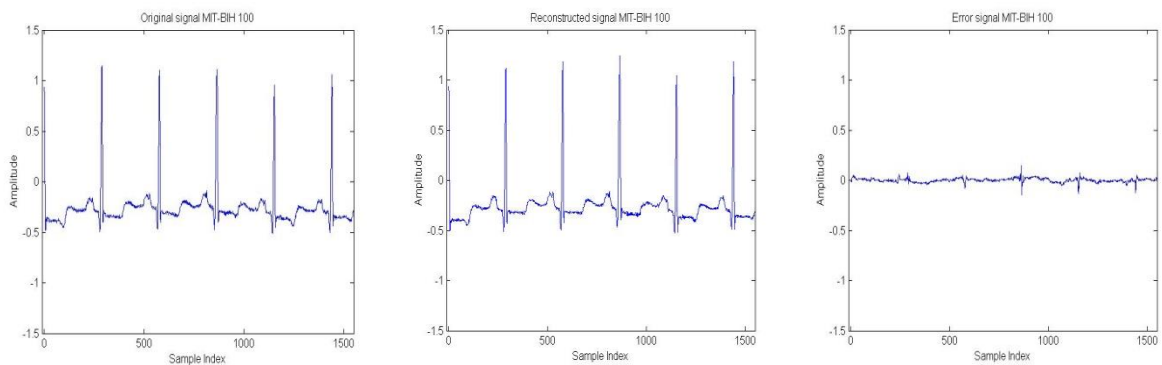
6.2 Experimental results of Algorithm I

Following the preprocessing steps described in 5.1, gain-shape VQ is applied. Gains of period-normalized signals are calculated by using (4.6), where $k = 8$. Through gain normalization, we have the shape signals. Both gains and shapes are vector quantized, where a $(8,8)$ vector quantizer is used for the shapes, $(36,6)$ vector quantizer for the gains, and $(8,3)$ vector quantizers for the difference signals in second stage. With this arrangement, we have $n_x = 11$ bps, $n_s = 1$ bps, $n_g = 0.02083$ bps, and $n_d = 0.375$ bps. When $k = 15$, vector quantizer for the shapes will be $(15,8)$, vector quantizers for the difference signals in second stage will be $(15,3)$. We have $n_x = 11$ bps, $n_s = 0.5333$ bps, and $n_d = 0.2$ bps.

Table 6.1 and Table 6.2 summarize the performance results of Algorithm I with $k = 8$ and $k = 15$. Original and reconstructed waveforms of MIT-100, MIT-119, MIT-122 are shown in Fig 6.1 to Fig 6.6.

Table 6.1 Performance results of Algorithm I

k	ECG sources	PRD(%)	CR
8	MIT-100	3.6636	7.88
	MIT-119	3.7763	7.88
	MIT-122	1.3248	7.88
15	MIT-100	6.3692	14.78
	MIT-119	6.2131	14.78
	MIT-122	2.3121	14.78

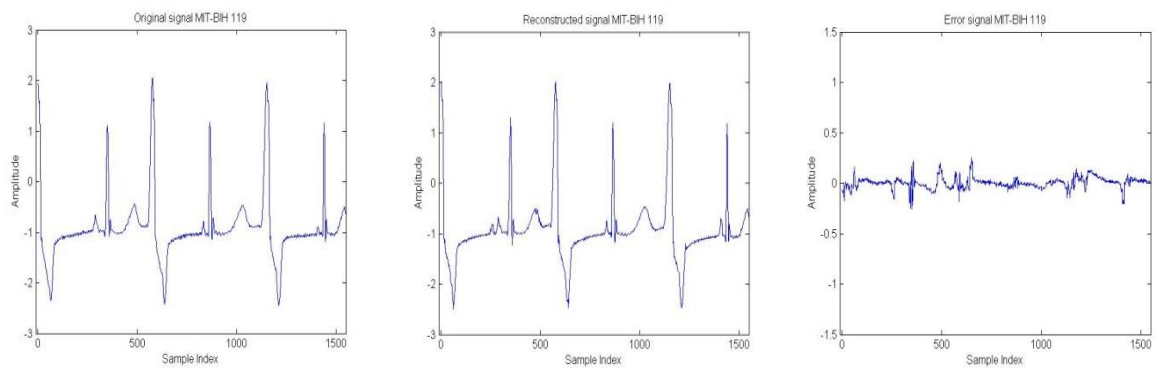


(a)

(b)

(c)

Figure 6.1 Results of Algorithm I ($k = 8$) in MIT-BIH 100: (a) original signal, (b) reconstructed ECG waveforms, and (c) error signals.



(a)

(b)

(c)

Figure 6.2 Results of Algorithm I ($k = 8$) in MIT-BIH 119: (a) original signal, (b) reconstructed ECG waveforms, and (c) error signals.

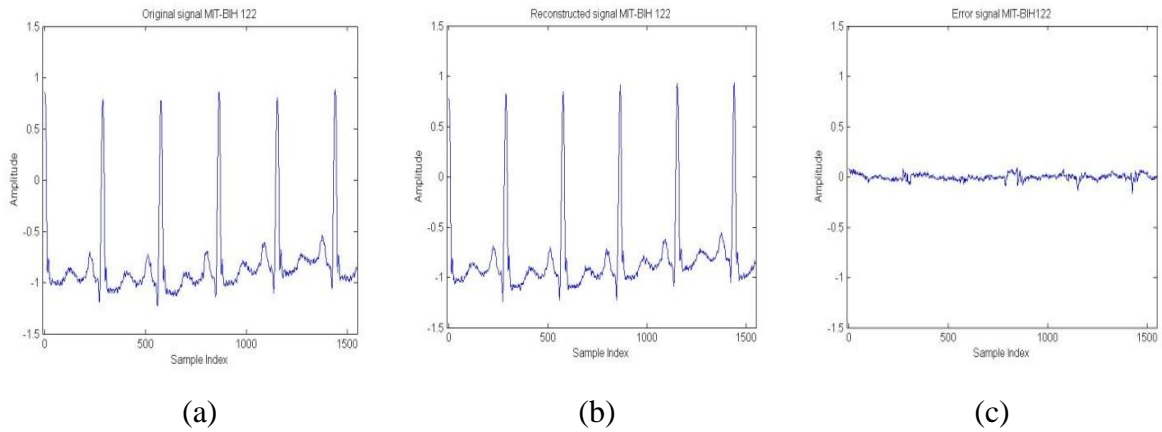


Figure 6.3 Results of Algorithm I ($k = 8$) in MIT-BIH 122: (a) original signal, (b) reconstructed ECG waveforms, and (c) error signals.

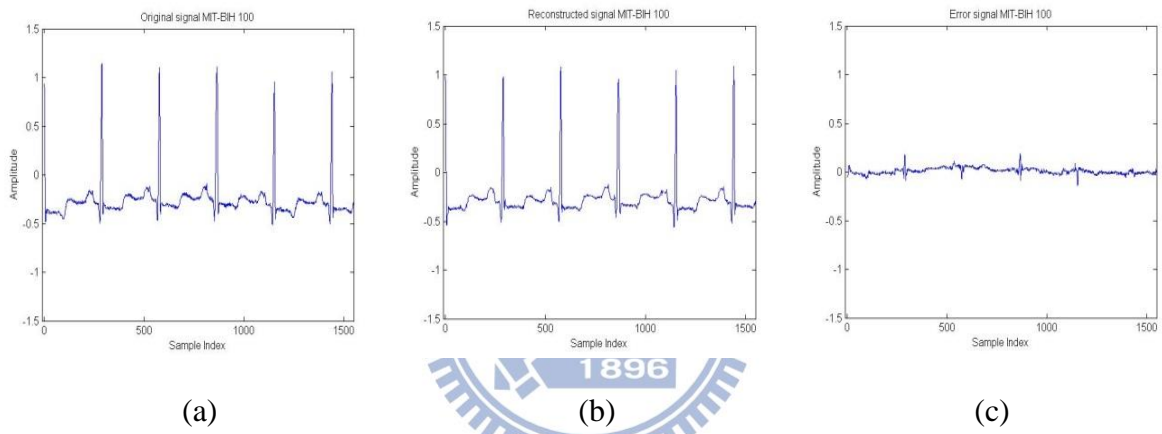


Figure 6.4 Results of Algorithm I ($k = 15$) in MIT-BIH 100: (a) original signal, (b) reconstructed ECG waveforms, and (c) error signals.

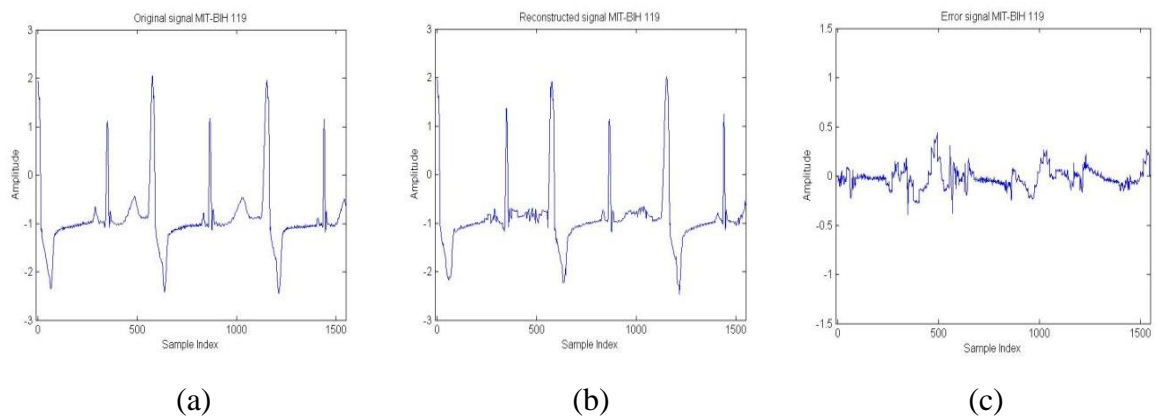


Figure 6.5 Results of Algorithm I ($k = 15$) in MIT-BIH 119: (a) original signal, (b) reconstructed ECG waveforms, and (c) error signals.

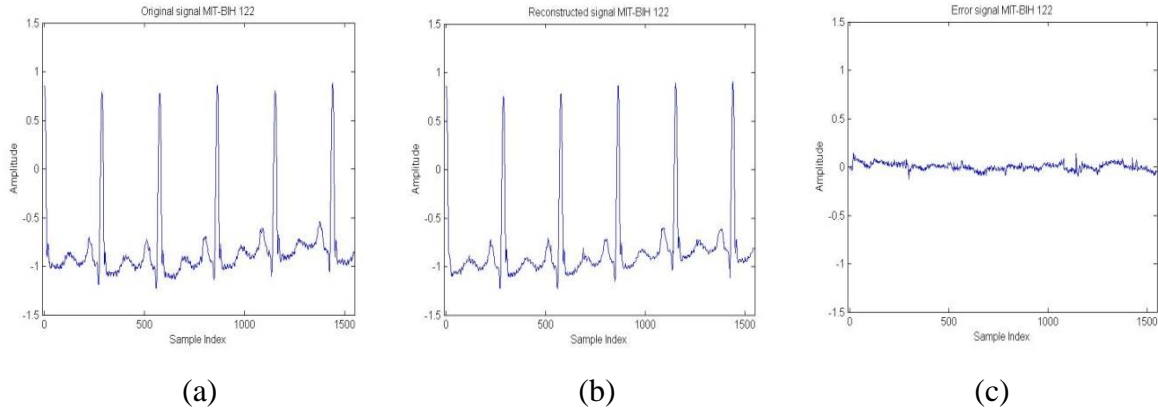


Figure 6.6 Results of Algorithm I ($k = 15$) in MIT-BIH 122: (a) original signal, (b) reconstructed ECG waveforms, and (c) error signals.

The results show that most reconstruction errors occur near the QRS complex. The reason is that most of the gain-normalized signals have low amplitude, implying that many low-amplitude vectors may exist in the shape codebook. However, the vectors representing the QRS complex are of high amplitude. When vector quantizing, these vectors are prone to being assigned indexes corresponding to low-amplitude signals. These errors cannot be well compensated even if gains are multiplied back.

6.3 Experimental results of Algorithm II

For this Algorithm, QRS complex detection and period normalization are applied for preprocessing as mentioned in 6.1. We used four datasets formed by taking the four records (MIT-100, MIT-108, MIT-119, MIT-122) from the MIT-BIH arrhythmia database. These datasets were chosen because they were used in earlier studies, and allow us to compare the performance of the proposed method with the Algorithm I. The four datasets are individual 10 min of data from the four records. PRD was used to evaluate the error between the original and the reconstructed ECG signals. The reported CR are from actual compressed files and include all side information required by the decoder. Modification of the proposed scheme is to achieve lossless decompression by utilizing the lossless compression capability of JPEG2000.

Table 6.3 summarizes the performance results of Algorithm II with PRD and CR evaluation. Original and after period-normalization matrixes are shown in Fig 6.7 – Fig 6.10. Fig 6.11- Fig 6.14 show original, reconstructed waveforms and error signals of the four datasets, respectively.

Table 6.2 Performance results of Algorithm II

ECG sources	PRD(%)	CR
MIT-100	3.0523	13.9534
MIT-108	6.4794	18.8851
MIT-119	2.6751	16.0050
MIT-122	1.6115	12.7506

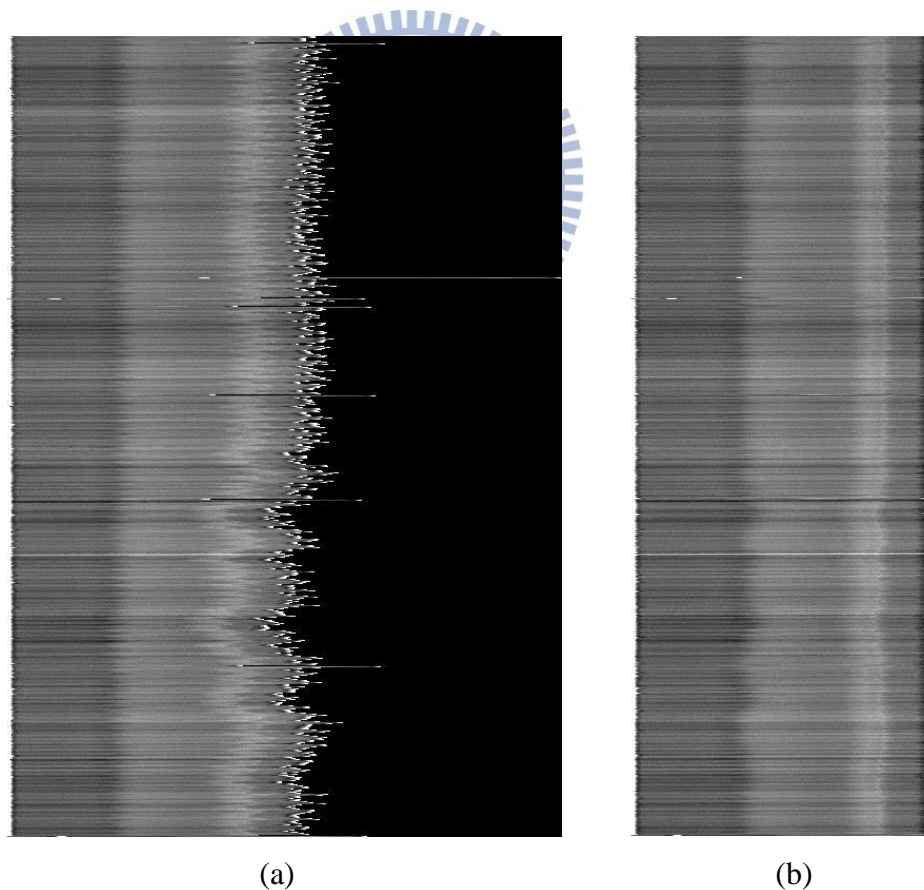
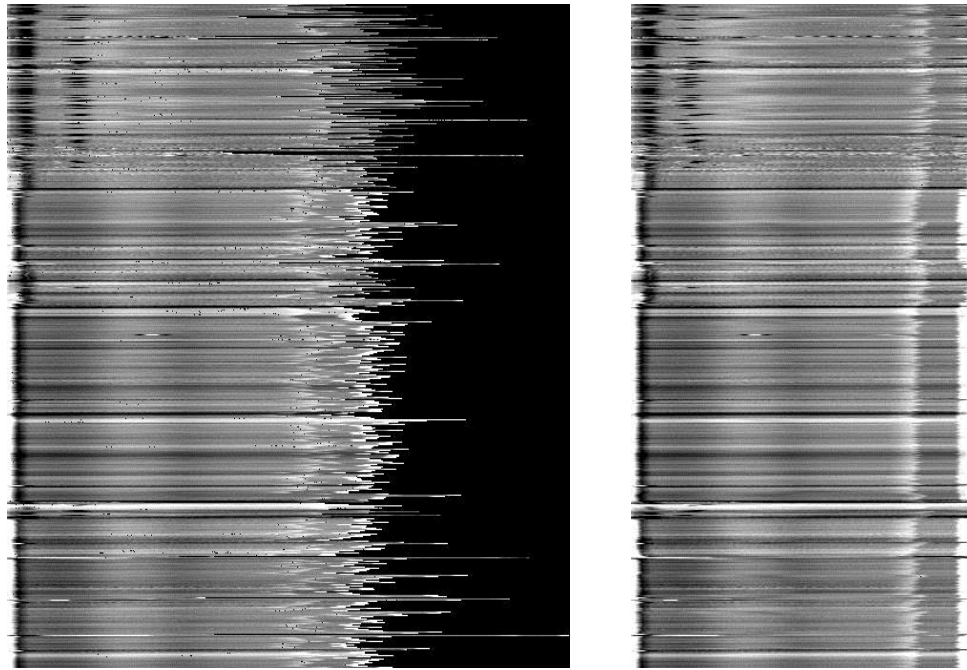


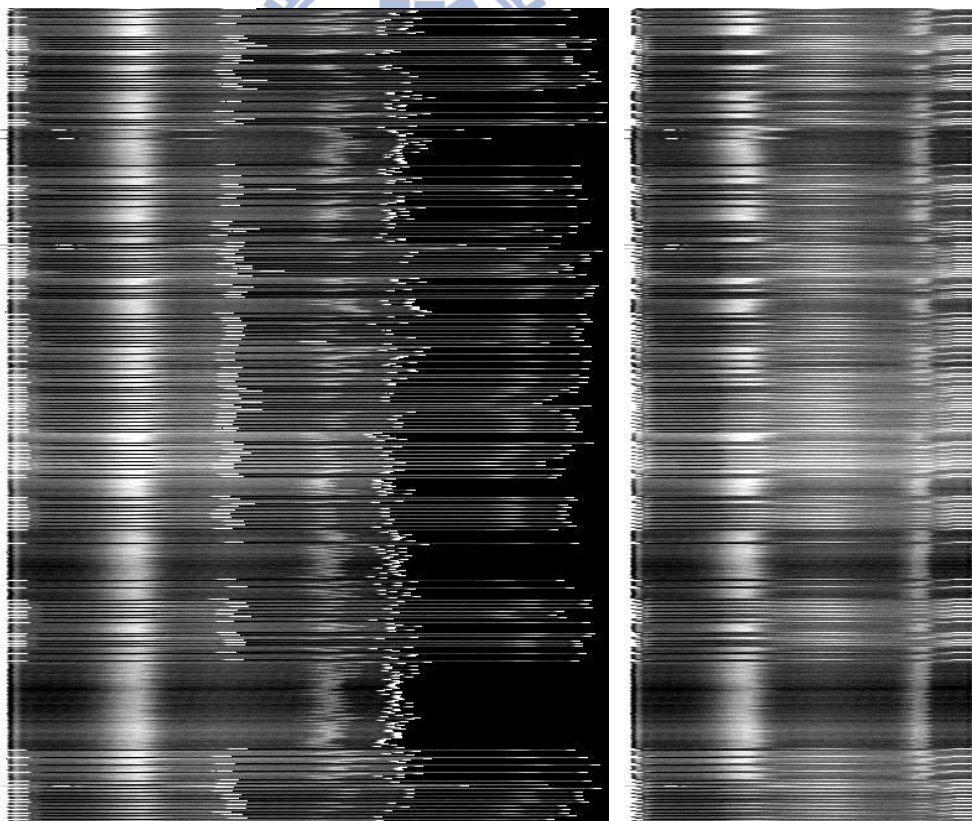
Figure 6.7 MIT-100:(a)Original matrixes, (b) After period-normalization matrixes



(a)

(b)

Figure 6.8 MIT-108: (a)Original matrixes, (b) After period-normalization matrixes



(a)

(b)

Figure 6.9 MIT-119: (a)Original matrixes, (b) After period-normalization matrixes

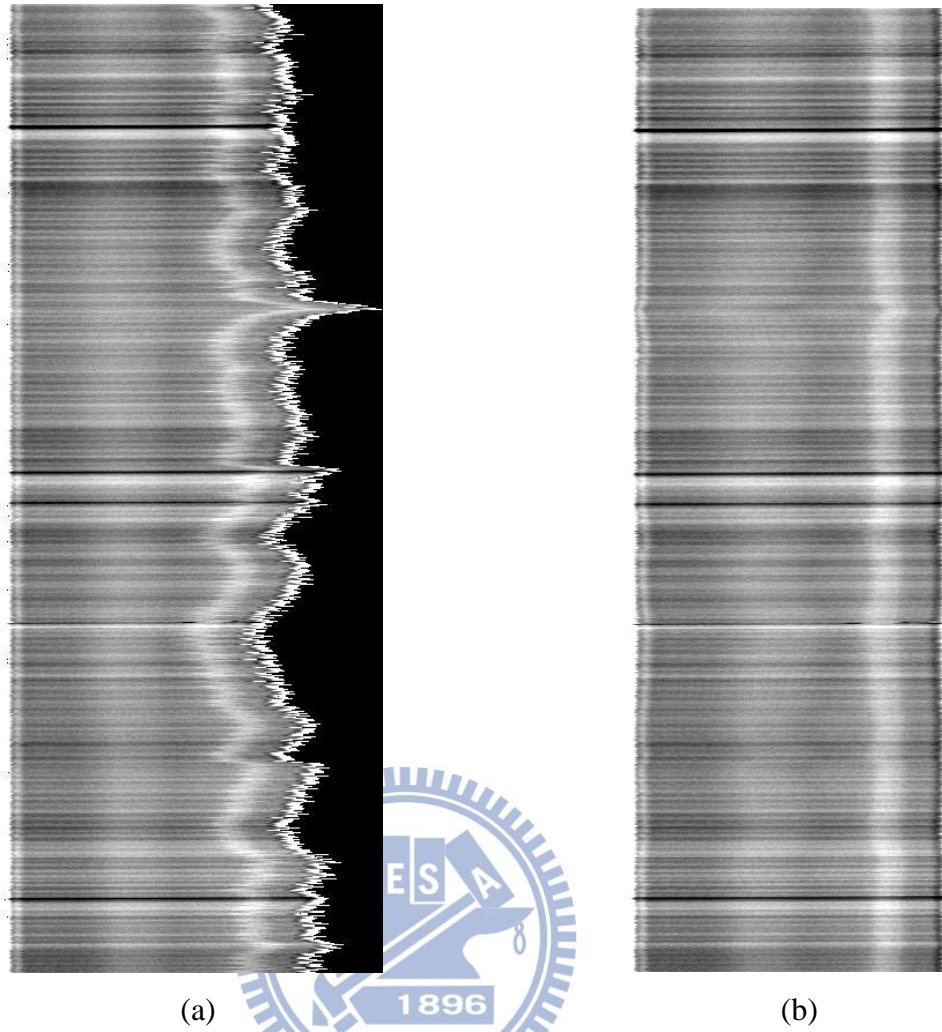


Figure 6.10 MIT-122: (a)Original matrixes, (b) After period-normalization matrixes

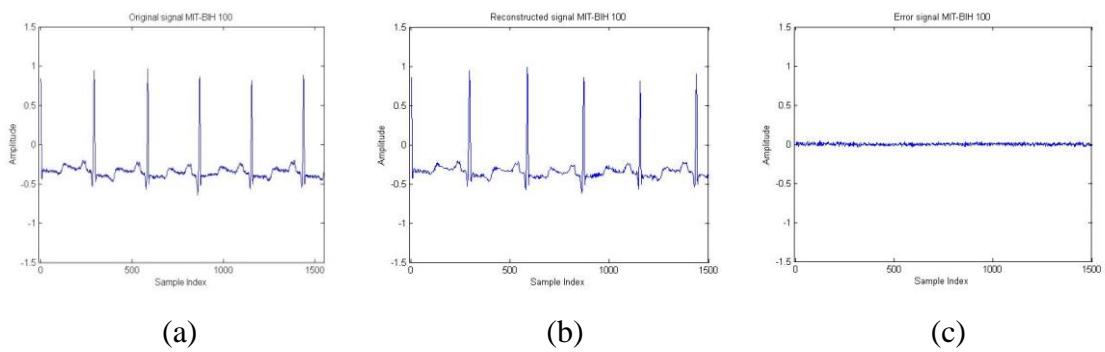


Figure 6.11 Results of Algorithm II in MIT-BIH 100:(a) Original signal,(b) Reconstructed ECG waveforms, and (c) Error signals.

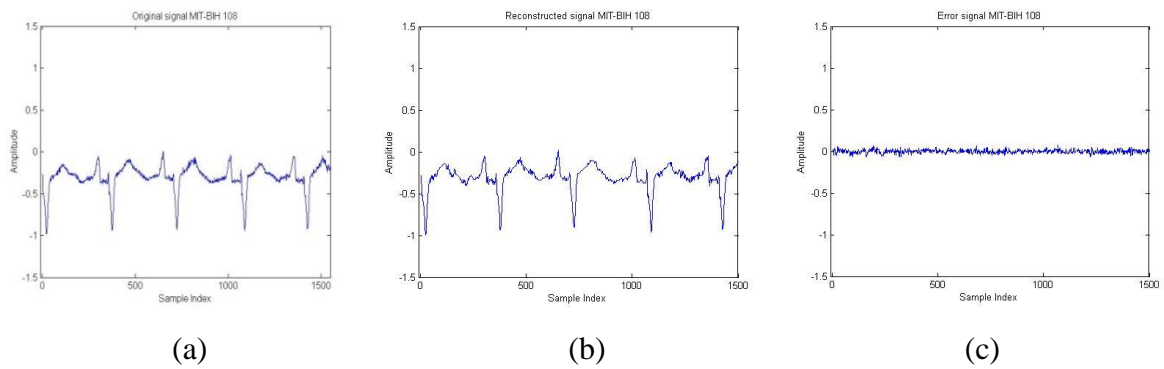


Figure 6.12 Results of Algorithm II in MIT-BIH 108: (a) Original signal,(b) Reconstructed ECG waveforms, and (c) Error signals.

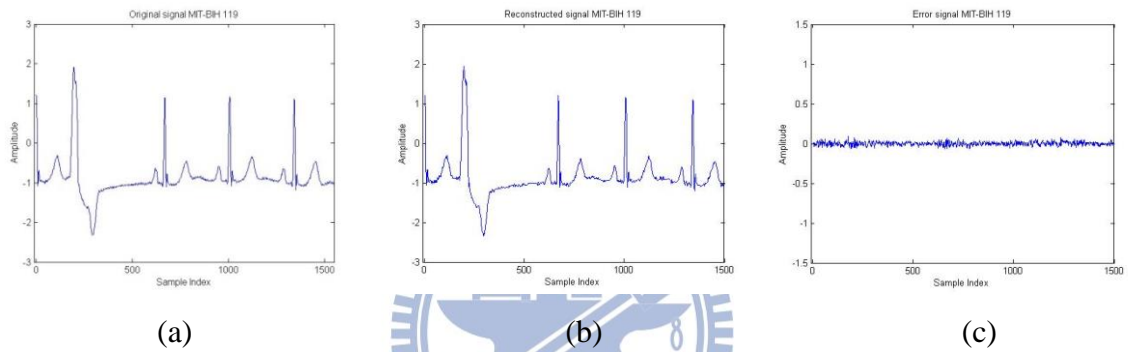


Figure 6.13 Results of Algorithm II in MIT-BIH 119: (a) Original signal,(b) Reconstructed ECG waveforms, and (c) Error signals.

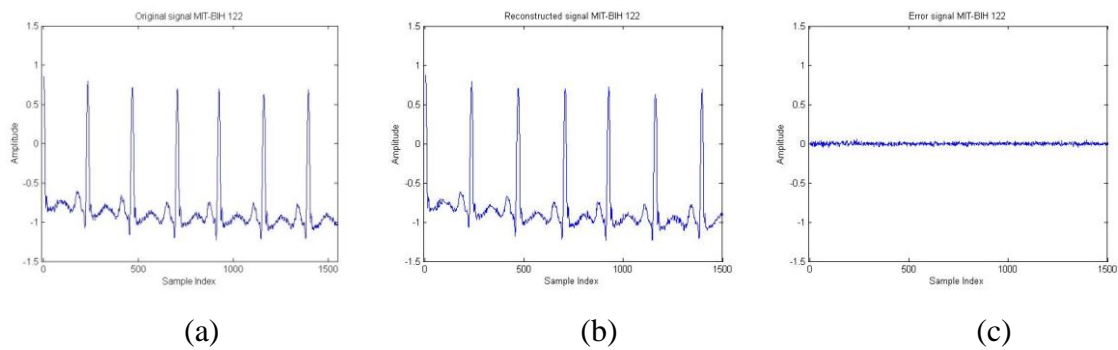


Figure 6.14 Results of Algorithm II in MIT-BIH 122: (a) Original signal,(b) Reconstructed ECG waveforms, and (c) Error signals.

6.4 Experimental results of ECG denoising

Signal de-noising in one dimension can be divided into three steps, including decomposition, threshold and signal reconstruction. When applying the HHT to ECG denoising, the key step is the empirical mode decomposition (EMD). A new filtering form (time-scale filtering) is constructed by using multi-revolution analysis and multi-scale filtering of EMD [24]. The advantage of the time-scale filtering is its ability to retain the inherent characteristics of the nonlinear and nonstationary signals. We use the EMD to break down the ECG signals into different time scales; which show different information of signal and noise. For ECG signal, noise and valuable information are mixed in IMF. Hard or soft threshold can be used in a similar way as wavelet transform threshold de-noising [25, 26]. Adaptive threshold values are given to each IMF. We add up all the new IMFs which remain after the threshold processing, and reconstruct the ECG signal. MIT-BIH 108 records are chosen for this experiment, since the signal is contaminated with high-frequency noise and baseline drift. Firstly, we perform EMD on the MIT-BIH 108 signal and obtain eight IMFs ranging from fine to coarse scale. They are IMF1 – IMF8 and its residue (RES) as shown in Fig 6.15. After the decomposition, we analyze each IMF according to the original data. It can be found that baseline drift is reflected in higher-standard scale, like IMF7 and IMF8. On the other hand, high-frequency noise is mainly in the lower scale of intrinsic mode function. The noise with 50HZ is also reflected in the lower scale. After that threshold process is carried out with the following steps:

- 1) The original ECG signal is decomposed with the EMD method;
- 2) A total of 8 IMFs scales are processed with soft thresholds in order to eliminate both high-frequency noise and noise with 50HZ;
- 3) Reconstruct the ECG-dominated signal with eight new IMFs.

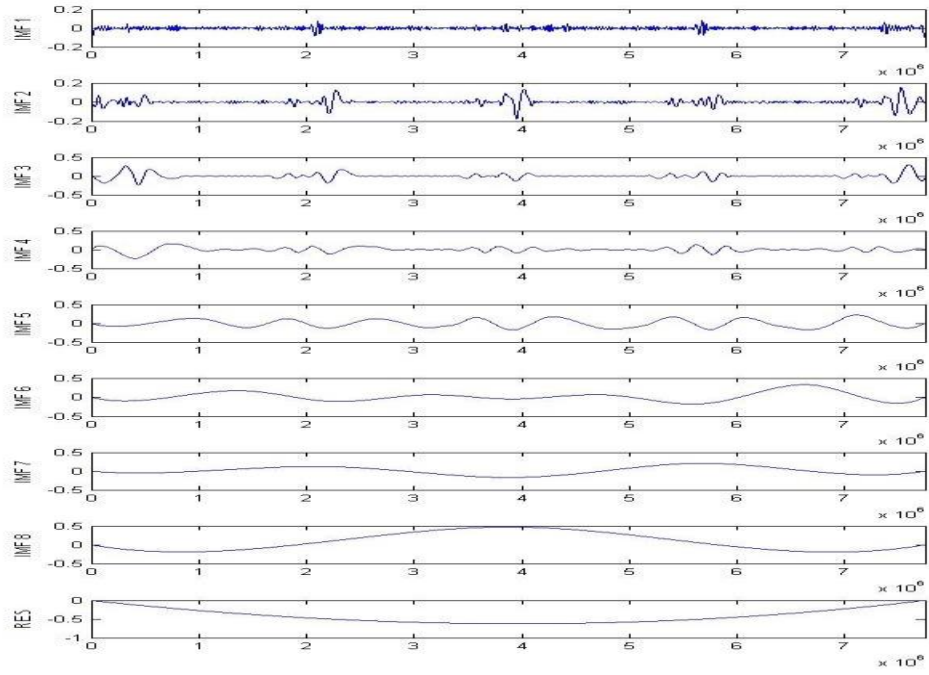


Figure 6.15 Eight intrinsic mode functions after empirical mode decomposition

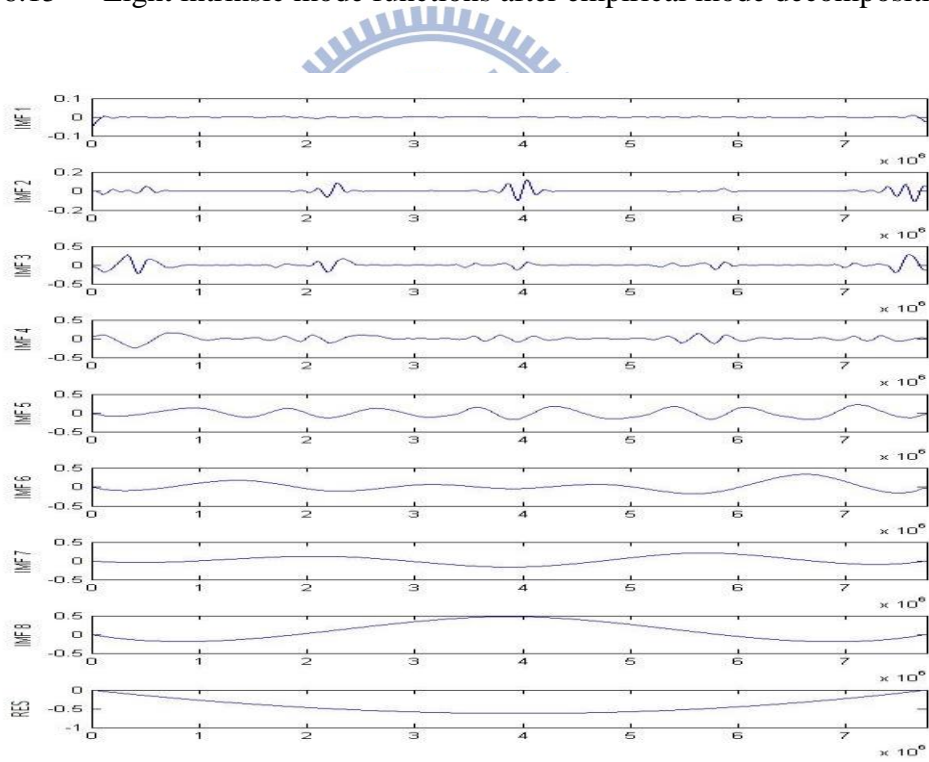


Figure 6.16 Eight intrinsic mode functions after applying soft threshold

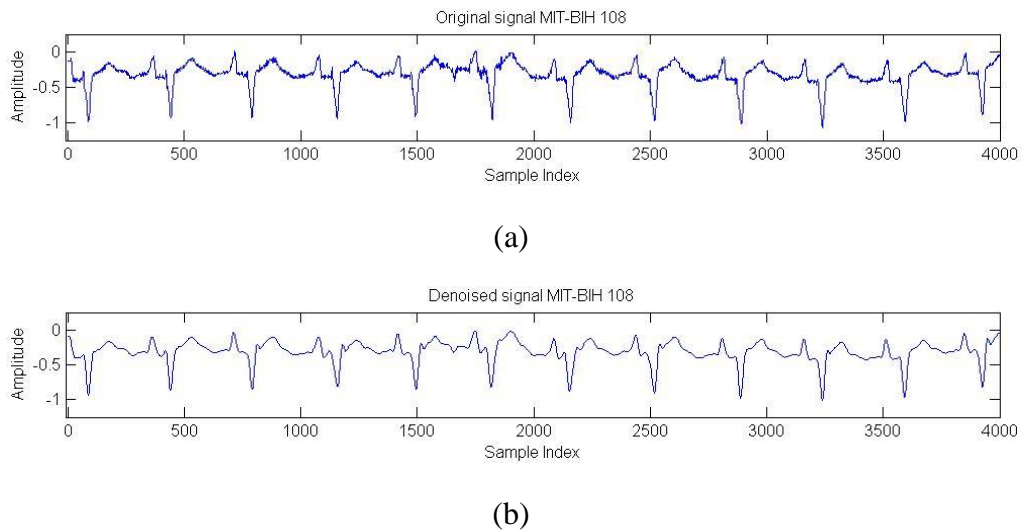


Figure 6.17 MIT-BIH 108:(a) Original signal, (b) Denoised signal

Fig6.17 shows the de-noising effect by using the HHT method. The results show that the HHT method can remain more valuable detail of signal. That is mainly because HHT method can make prevention of energy leak and the energy is more centralized in spectrum. The EMD is multi-scale filtering which can effectively remove noise. Finally we have the following conclusions by comparison:

- 1) Both HHT and wavelet transform can be used to analyze nonstationary signal and thus achieve the desired effect of de-noising.
- 2) The EMD is adaptive, since the basic functions extracted from original data are based on residue of the last filtering, which are alterable in HHT.
- 3) Alterable amplitude and instantaneous frequency can improve the efficiency of decomposition. Amplitude and frequency are distinct during EMD and therefore the fitting for amplitude and frequency are not required.

Chapter 7 Conclusions

Goal of this thesis is to develop noise-resilient ECG signal compression methods. We first introduce the basic of HHT theorem and its application to signal denoising. JPEG2000 is used for its two-dimensional of ECG signals. To implement this, one-dimensional ECG signals are transformed to two-dimensional representations by two preprocess, including QRS complex detection and period normalization. The two preprocesses are used to maximize the inter-beat correlation. In order to reduce the computation of VQ codebook search, we also investigate a multiple stage scheme (MSVQ). Experimental result shows that the proposed algorithms achieve good reconstruction quality with high compression ratio.

Some possible future directions in this research are listed as follows.

1. Backward gain-adaptive VQ is an attractive way to model the ECG correlation without extra cost of gain-related side information. Other gain estimators may also be investigated to achieve better performance when GSVQ and MSVQ is applied.

2. In this work, because of the inconsistency of heartbeat lengths, a period normalization process is needed. Continuing our research, we will address ourselves to the study of designing a better ECG compression algorithm utilizing the inter-beat correlation without miscellaneous preprocessing

3. The proposed scheme achieves lossless decompression by utilizing JPEG2000 on single signal. How to use the multi-component capabilities of JPEG2000 to compress multichannel ECG data are also topics for future research.

Bibliography

- [1] A. Gersho, "On the structure of vector quantizers," IEEE Trans. Inform. Theory, vol. IT-28, pp. 157-166, Mar. 1982.
- [2] J. P. Adoul, C. Collin, and D. Dalle, "Block encoding and its application to data compression of PCM speech," in Proc. Canadian Commun. EHV Conf., Montreal, P.Q., Canada, 1978, pp. 145-148.
- [3] D. T. S. Chen, "On two- or more dimensional optimum quantizers," in Proc. IEEE Int. Conf. Acoust., Speech, Signal Processing,
- [4] A. Gersho, "Asymptotically optimal block quantization," IEEE Trans. Inform. Theory, vol. IT-25, pp. 373-380, July 1979.
- [5] S. P. Lloyd, "Least-squares quantization in PCM," IEEE Trans. Inform. Theory, vol. IT-28, pp. 129-137, Mar. 1982.
- [6] Linde, Y., Buzo, A., Gray, R.M., An Algorithm for Vector Quantizer Design, IEEE Transactions on Communications, vol. 28, pp. 84-94, 1980.
- [7] -, "Classified vector quantization of images," IEEE Trans. Commun., vol. COM-34, pp. 1105-1115, Nov. 1986.
- [8] S. P. Lloyd, "Least-squares quantization in PCM," IEEE Trans. Inform. Theory, vol. IT-28, pp. 129-137, Mar. 1982
- [9] Y. Linde, A. Buzo, and R. M. Gray, "An algorithm for vector quantizer design," IEEE Trans. Commun., vol. COM-28, pp. 84-95, Jan. 1980.
- [10] A. Buzo, A. H. Gray, Jr., R. M. Gray, and J. D. Markel. Speech coding based upon vector quantization. IEEE Trans. Acoust. Speech Signal Process., ASSP-28:562-574, October 1980.
- [11] M. J. Sabin and R. M. Gray. Product code vector quantizers for waveform and voice coding. IEEE Trans. Acoust. Speech Signal Process., ASSP-32:474-488, June 1984.
- [12] B.-H. Juang and A. H. Gray, Jr. Multiple stage vector quantization for speech coding. In International Conference on Acoustics, Speech, and Signal Processing, volume 1, pages 597-600, Paris, April 1982.
- [13] C. F. Barnes and R. L. Frost. Necessary conditions for the optimality of residual vector quantizers. In Abstracts of the 1990 IEEE International Symposium on Information Theory, page 34, San Diego, Calif., January 1990.

- [14] R. L. Frost, C. F. Barnes, and F. Xu. Design and performance of residual quantizers. In J. A. Storer and J. H. Reif, editors, Proceedings Data Compression Conference, pages 129-138, Snowbird, Utah, April 1991. IEEE Computer Society Press.
- [15] D. Taubman, "High Performance Scalable Image Compression With EBCOT", Proc. IEEE Int. Conference Image Processing, Vol.III, pp. 344-348, Kobe, Japan, October 1999.
- [16] D. Taubman, "High Performance Scalable Image Compression With EBCOT", IEEE Trans. Image Processing, Vol. 9, No. 7, pp. 1158-1170, July 2000.
- [17] Charilaos Christopoulos¹, Athanassios, and TouradjEbrahimi, THE JPEG2000 STILL IMAGE CODING SYSTEM: AN OVERVIEW Published in IEEE Transactions on Consumer Electronics, Vol. 46, No. 4, pp. 1103-1127, November 2000
- [18] J.-J. Wei, C.-J. Chang, N.-K. Chou, and G.-J. Jan, "ECG data compression using truncated singular value decomposition", IEEE Trans. on Information Technology in Biomedicine, vol. 5, pp. 290-299, Dec. 2001.
- [19] T. M. Lehman, C. Gonner, and K. Spitzer, "Survey: interpolation methods in medical image processing", IEEE Trans. on Medical Imaging, vol. 18, pp. 1049-1075, Nov. 1999.
- [20] N.E.Huang, "The empirical mode decomposition and Hilbert spectrum for nonlinear and nonstationary time series analysis", Pro.R.Soc, London, 1998, 454, pp. 903-995.
- [21] DONOHO D L."De-noising by Soft-thresholding[J]". IEEE Trans.Inform,Theory,1995, 41 (3) : 613 - 627 .
- [22] D.L. Donoho and LM. Johnston, " Spatial adaptation via wavelet shrinkage",Biometrika, vol. 81, 1994, pp 425-455.
- [23] D.L. Donoho and LM. Johnston, "Adapting to unknown smoothness via wavelet shrinkage", J. of the American Statistical Association, vol.90, 1995, pp 1200-1224.
- [24] Wang Chun, Peng Dong-ling, "The Hilbert-Huang Transform and Its Application on Signal De-noising", China Journal of Scientific Instrument, 2004, Vol.25,no.4, pp. 42-45.
- [25] Ji Hu, Sun Ji-xiang, "De-noising of ECG signal based on discrete stationary wavelet transform", Computer Application, 2005, Vol.25, no.6, pp. 1318-1320.
- [26] Gao Qing-wei, Li Hai-ying, "De-noising of ECG signal based on stationary wavelet transform", Acta Electronica Sinica, 2003, Vol.31, no.2, pp. 238-240.
- [27] A. Bilgin, M. W. Marcellin, and M. I. Altbach, "Compression of Electrocardiogram Signals Using JPEG2000," IEEE Transactions on Consumer Electronics, vol. 49, no. 4, pp. 833-840, 2003.

- [28] H.H. Chou, Y.J. Chen, Y.C. Shiau, and T.S. Kuo, "An Effective and Efficient Compression Algorithm for ECG Signals with Irregular Periods," IEEE Transactions on Biomedical Engineering, vol. 53, no. 6, pp. 1198-1205, 2006.

